

Academic Year
2022 - 2023

Evaluation of the Immunogenicity of a Novel
Combination Strategy for Head and Neck Squamous
Cell Carcinoma in 3D Tumor Models
Innovative Non-Thermal Plasma with Standard of Care Cisplatin

Mauranne Bauwens

Educational Commission Biomedical Sciences

**Master thesis in partial fulfillment of the requirements for the degree
Master of Biomedical Sciences: Molecular Mechanisms of Diseases**

Promotor(s)

Dr. Abraham Lin

Co-promotor

Hanne Verswyvel

Coach

Hanne Verswyvel

Center for Oncological Research (CORE) in collaboration with PLASMANT

Campus Drie Eiken, Universiteitsplein 1, Building T floor 4, 2610 Wilrijk

Table of Contents

1	Acknowledgments	iii
2	List of Abbreviations	iv
3	English Abstract	vi
4	Nederlandstalig Abstract	vii
5	Introduction	1
5.1	<i>Head and Neck Squamous Cell Carcinoma</i>	1
5.1.1	Introduction to the Disease	1
5.1.2	Drawbacks of Current Standard Treatment Strategies	2
5.2	<i>The Cancer-Immunity Cycle and Immunogenic Cell Death</i>	2
5.2.1	The Cancer-Immunity Cycle as Therapeutic Target	2
5.2.2	Immunogenic Cell Death Induction as Promotor of the Cancer-Immunity Cycle	4
5.3	<i>Non-Thermal Plasma</i>	5
5.3.1	The Anti-Cancer Activity of Non-Thermal Plasma	5
5.4	<i>3D Tumor Models to Better Mirror the Tumor Microenvironment</i>	6
5.4.1	The Limitations of 2D Cell Cultures	6
5.4.2	The Appearance of the Complex Tumoral Setting	6
5.4.3	The Current and Future Successes of 3D Cell Cultures	6
6	Aims and Objectives	8
7	Materials and Methods	9
7.1	<i>Cell Cultures</i>	9
7.2	<i>3D Spheroid Tumor Model</i>	9
7.3	<i>NTP-CIS Double Treatment Strategy</i>	9
7.3.1	NTP with DBD Device	9
7.3.2	Cisplatin Treatment	10
7.4	<i>Agarose Embedding and Preparation of Microscopic Slides</i>	11
7.5	<i>Immunofluorescence and Imaging</i>	11
7.6	<i>ATP Secretion</i>	12
7.7	<i>HMGB1 Release</i>	12
7.8	<i>Co-Culture of HNSCC Spheroids with Monocyte-Derived Dendritic Cells</i>	13
7.8.1	Generation of Monocyte-Derived IDCs and Green-Fluorescent Spheroids (Day 1-4)	13
7.8.2	DC Co-Culture and Flow Cytometric Analysis of Maturation and Phagocytosis (Day 5-7)	14
7.8.3	Gating Strategy	14
7.9	<i>Establishment of Organoid Culture from Fresh Tumor Sample</i>	15
7.10	<i>Organoid Sub-Culturing and Experimental Preparation</i>	16
7.11	<i>Harvesting and Experimental Handling of Organoids</i>	17
7.12	<i>Statistical Analysis</i>	17
8	Results	18

8.1	<i>Surface-Presented DAMPs Increased After NTP-CIS Combination Therapy</i>	18
8.2	<i>ATP Secretion Increased After NTP Monotherapy</i>	20
	21
8.3	<i>HMGB1 Release Increased Following Combined NTP-CIS Therapy</i>	21
8.4	<i>NTP-CIS Combination Therapy Improved DC Phagocytosis and Expression of Activation and Maturation Markers</i>	22
8.5	<i>Patient-Specific Therapy Response Validated in HNSCC Organoids</i>	26
9	Discussion	28
10	Supplementary Material	31
10.1	<i>Organoid Medium</i>	31
11	Literature references	a

1 Acknowledgments

Last 6 months were marked by gaining hopes of knowledge, a lot of experimental work, and many ‘exciting puppy’ feelings due to the live experience of science. Thereby, I would like to express my gratitude to everyone that contributed to this journey.

First of all, I would like to offer my sincere thank you to all members of the Center for Oncological Research (CORE). I’m grateful for having the opportunity to work with such an openhearted and talented team. I appreciate every bit of help, shared knowledge, and motivation that I have received from you over the past few months. It was an honor to contribute to your research and especially to be part of your team.

I would like to deeply thank Prof. Dr. Evelien Smits for the opportunity to conduct my master thesis at CORE and for welcoming me in the Solid Tumor Immunology Group (STIG). Furthermore, I am grateful to Prof. Dr. Annemie Bogaerts for the collaboration with PLASMANT and introducing me to the (previously unknown to me) application of plasma within the oncology field.

Hereafter, my special thank you to my promotor Dr. Abraham Lin for the constructive feedback, insights, and evaluation of my work. Also, thanks to challenge me in thinking in new and innovative ways and for having the brainstorm sessions! I admire how at home you are in every scientific subject.

My deepest gratitude and appreciation go to my co-promotor and coach Hanne Verswyvel. Thank you for teaching me a variety of different techniques, helping me develop my writing skills, and showing me so many different aspects of the research world. I appreciate our good communication and the feeling of ‘teamwork’, although you taught me to work independently and to believe in my capacities more. I am glad you pushed me sometimes to get out of my comfort zone and structured, planned lifestyle. Thanks to you I was able to develop myself both professionally and personally. I couldn’t have imagined myself a better mentor than you.

Besides my experimental work, I also had the opportunity to attend a head and neck surgery, thanks to Gilles Van Haesendonck. In addition to my academic molecular-tinted background, this allowed me to learn a lot about the clinical discipline, contributing to my ‘translational bigger picture’.

I would like to thank my co-readers Prof. Dr. Jean-Pierre Timmermans and Prof. Dr. Tom Vanden Berghe for the feedback on my project proposal and the evaluation of my master thesis.

Finally, a big thank you to my parents, sister, friends, and boyfriend for being my forever biggest support. Thanks for the encouraging words, listening to my simplified scientific explanations, and always being there for me.

The dream of contributing to the fight against cancer has become reality and I can’t wait to see what the future holds. Many thanks to all of you!

Mauranne

2 List of Abbreviations

HNSCC	Head and neck squamous cell carcinoma
OPSCC	Oropharyngeal squamous cell carcinoma
HPV	Human papillomavirus
R/M	Recurrent or metastatic
CIS	Cisplatin
ICI	Immune checkpoint inhibitor
PD-L1	Programmed cell death ligand 1
CPS	Combined positive score
Ag	Antigen
APC	Antigen presentation
i/mDC	Immature/mature dendritic cell
CD	Cluster of differentiation
MHC	Major histocompatibility complex
TCR	T cell receptor
TGF-β	Transforming growth factor beta
ICD	Immunogenic cell death
DAMP	Damage-associated molecular pattern
PRR	Pattern recognition receptor
NK	Natural killer
CRT	Calreticulin
HSP	Heat shock protein
ATP	Adenosine triphosphate
HMGB1	High mobility group box 1
ER	Endoplasmic reticulum
TLR4	Toll-like receptor 4
NTP	Non-thermal plasma
RONS	Reactive oxygen and nitrogen species
DBD	Dielectric barrier discharge
2D	Two-dimensional
TME	Tumor microenvironment
ECM	Extracellular matrix
IC₅₀	Inhibitory concentration
3D	three-dimensional
CAF	Cancer-associated fibroblast
PBMC	Peripheral blood mononuclear cell
PDO	Patient-derived organoid

DMEM	Dulbecco's Modified Eagle Medium
FBS	Fetal Bovine Serum
ULA	Ultra-low attachment
Msp	Microsecond-pulsed
PFA	Paraformaldehyde
TBS	Tris-buffered saline
ELISA	Enzyme linked immune sorbent assay
RPMI	Roswell Park Memorial Institute
GM-CSF	Granulocyte macrophage colony stimulating factor
IL	Interleukin
TNF-α	Tumor necrosis factor alpha
PGE 2	Prostaglandin E2
FSC	Forward scatter
SSC	Side scatter
MFI	Mean fluorescence intensity
SEM	Standard error mean
BSA	Bovine serum albumin
IFN	Interferon
CAR-T	Chimeric antigen receptor therapy

3 English Abstract

Head and neck squamous cell carcinoma (HNSCC) is the 6th most common cancer type worldwide. The majority of patients is diagnosed in the advanced stages (~60%), wherein the disease is extremely challenging to treat, and patients often face relapse or metastasis (R/M HNSCC). Despite first-line immunotherapy, with or without chemotherapy (e.g., cisplatin (CIS)), prognosis remains poor (6-15 months). Moreover, it displays limited benefit due to low response rates and severe side effects in already weakened patients. Hence, there is a major need for new therapeutic strategies to improve treatment efficacy and tackle shortcomings, while supporting the patient's quality of life.

The immune system has an intrinsic defensive mechanism against malignancies, called “the cancer-immunity cycle”, a series of immune-activating events to elicit a prompt anti-tumoral response. In cancer patients, the cycle is interrupted and will subsequently fail in tumor elimination. However, this immune imbalance seems to be reversible, making cycle restoration an interesting target for therapeutic intervention (e.g., immunotherapy). In that regard, immunogenic cell death (ICD) induction is currently intensively investigated. This strategy stimulates the front-end part of the cancer-immunity cycle, via the release of damage-associated molecular patterns (DAMPs), through which further cycle effects may accumulate. Several standard of care therapies, including chemotherapy (e.g., low-dose CIS) have been reported to induce ICD. Other emerging treatments, like non-thermal plasma (NTP), have been evaluated over the last years for these immunogenic properties.

NTP is an ionized gas, generated at room temperature and atmospheric pressure, that consists of reactive oxygen and nitrogen species (RONS). Both *in vitro* and *in vivo* studies have demonstrated its anti-tumor capacity, with the NTP-produced short-lived RONS as the main drivers of ICD induction. So far, no clinical side effects have been reported. So, NTP shows immune-engaging and anti-cancer potential, tolerable in already weakened patients.

As both innovative NTP and HNSCC standard of care CIS demonstrated ICD induction in monotherapy, we hypothesized that a combined NTP-CIS application may amplify the immune-stimulatory treatment effects, including increased tumor immunogenicity. Therefore, **the goal of this study was to elucidate the immunogenicity of a novel NTP-CIS combination strategy, by evaluation of DAMP release and immune cell functionality in advanced 3D tumor models for HNSCC, in the interest of improved clinical response and efficacy of current standard of care therapies.**

To circumvent 2D limitations, we implemented three-dimensional (3D) culturing techniques to better represent the tumor microenvironment (TME) and intercellular interactions. A 3D spheroid tumor model was established for 3 HNSCC cell lines, Cal27, SCC22B, and SCC61, to evaluate ICD. Several ICD hallmarks were quantified: the membrane markers calreticulin (CRT), and heat shock proteins 70 and 90 (HSP70/90) were assessed by immunofluorescent imaging, whereas adenosine triphosphate (ATP) and high mobility group box 1 (HMGB1) in the supernatant were examined via a bioluminescent assay and an ELISA, respectively. Thereafter, the effects of increased immunogenicity on immune cells following NTP-CIS combination were functionally tested by co-culture experiments with monocyte-derived dendritic cells (DCs). DC phagocytosis, and maturation and activation were evaluated using flow cytometry. Finally, the highly-advanced patient-derived organoid (PDO) model was implemented to characterize NTP-CIS treatment effects on organoid survival, to validate our previous findings in HNSCC spheroids.

Our data showed a significant upregulation of cell-surface CRT, an important ‘eat-me signal’ for immune cells, along with the chaperones HSP70 and HSP90. In addition, NTP therapy improved the release of both the early ICD marker ATP, as the late-stage factor HMGB1. Evaluating immune cell function, DC co-culture experiments demonstrated increased HNSCC tumor cells phagocytosis after NTP-CIS combined application, suggesting better immune recognition. These results highlight the potential of NTP to enhance treatment efficacy and tumor immunogenicity, especially in the combinatorial setting with standard of care agents. Lastly, preliminary organoid survival data confirmed a higher tumor killing after the application of both NTP and CIS.

In summary, the goal of this project was to gain a deeper understanding of the HNSCC immunogenicity after NTP-CIS combination therapy. Hence, we demonstrated that this promising application supported the front-end part of the cancer-immunity cycle via ICD-induced DAMP release. By increasing immunogenicity, the back-end of the cycle may be promoted, and subsequently result in a systemic and long-lasting immune response.

Hence, our results will potentially accelerate clinical translation and are a pivotal step towards a rationally-designed combination strategy with NTP to improve current first-line HNSCC therapies.

4 Nederlandstalig Abstract

Hoofd-hals plaveiselcelcarcinoom (HNSCC) is het 6^e meest voorkomende kankertype wereldwijd. De meeste patiënten worden gediagnosticeerd in vergevorderd stadia (~60%), waarbij de ziekte extreem moeilijk te behandelen is en patiënten vaak te maken krijgen met recidief of metastase (R/M HNSCC). Ondanks eerstelijns immuuntherapie, met of zonder chemotherapie (bv. cisplatine (CIS)), blijft de prognose slecht (6-15 maanden). Tevens zijn de voordelen beperkt door de lage respons en ernstige bijwerkingen bij reeds verzwakte patiënten. Daarom is er grote behoefte aan nieuwe therapeutische strategieën om de behandelingsdoeltreffendheid te verbeteren en de gebreken aan te pakken, en tegelijkertijd de levenskwaliteit van de patiënten te ondersteunen. Het immuunsysteem heeft een intrinsiek verdedigingsmechanisme tegen maligniteiten, genaamd "de kanker-immuniteitscyclus", een reeks immuun-activerende stappen om snelle antitumorale respons uit te lokken. Bij kankerpatiënten is deze cyclus ontregeld waardoor tumoreliminatie mislukt. Deze immuun-disbalans lijkt echter omkeerbaar te zijn, met cyclusherstel als boeiend doelwit voor therapeutische interventie (bv. immuuntherapie). In dat opzicht wordt immunogene celdood (ICD) inductie intensief onderzocht. Deze strategie stimuleert het eerste deel van de kanker-immuniteitscyclus via vrijgave van "schade-geassocieerde moleculaire patronen" (DAMPs), waardoor verdere cycluseffecten accumuleren. Verschillende standaardtherapieën, waaronder chemotherapie (bv. CIS in lage dosis), toonden al ICD inductie aan. Andere opkomende behandelingen, zoals niet-thermisch plasma (NTP), zijn de afgelopen jaren geëvalueerd op deze immunogene eigenschappen.

NTP is een geïoniseerd gas, gegenereerd bij kamertemperatuur en atmosferische druk, dat reactieve zuurstof- en stikstofspecties (RONS) bevat. Zowel *in vitro* als *in vivo* studies hebben anti-tumor capaciteit aangetoond, tot op heden zonder klinische bijwerkingen, met de NTP-geproduceerde kortlevende RONS cruciaal in ICD inductie. NTP toont dus een immuun-stimulerend en kanker-bestrijdend potentieel, verdraagbaar bij verzwakte patiënten. Aangezien zowel innovatieve NTP als HNSCC standaardbehandeling CIS ICD inductie aantoonde in monotherapie, stelden wij de hypothese dat de combinatie van NTP-CIS de immuunstimulerende behandelingseffecten kan versterken, inclusief verhoogde tumor immunogeniciteit. Daarom was **het doel van deze studie het ophelderen van de immunogeniciteit van een nieuwe NTP-CIS combinatiestrategie, door evaluatie van DAMP afgifte en immuuncel functionaliteit in geavanceerde 3D tumormodellen voor HNSCC, in het belang van verbeterde klinische respons en werkzaamheid van de huidige standaardtherapieën.**

Om de 2D-beperkingen te omzeilen, implementeerden we driedimensionale (3D) kweektechnieken om de tumormicro-omgeving (TME) en intercellulaire interacties beter weer te geven. Een 3D-sferoïd tumormodel werd gemaakt van 3 HNSCC cellijnen, Cal27, SCC22B en SCC61, voor ICD evaluatie. Verschillende ICD kenmerken werden gekwantificeerd: de membraan-markers calreticuline (CRT) en hiteschok eiwitten 70 en 90 (HSP70/90) werden beoordeeld met immunofluorescentie, terwijl adenosinetrifosfaat (ATP) en high mobility group box 1 (HMGB1) in het supernatant onderzocht werden met respectievelijk een bioluminescentietest en ELISA. Daarna werden de effecten van verhoogde immunogeniciteit op immuuncellen na NTP-CIS combinatie functioneel getest door co-cultuurexperimenten met monocyt-afgeleide dendritische cellen (DCs). DC fagocytose, maturatie en activatie werden geëvalueerd met flowcytometrie. Tot slot werd het zeer geavanceerde patiënt-afgeleide organoïde (PDO) model geïmplementeerd om de effecten van NTP-CIS behandeling op organoïden overleving te karakteriseren, om onze eerdere sferoïden bevindingen te valideren.

Onze resultaten toonden een significante opregulatie in celoppervlakte CRT, een 'eet-me-signaal' naar immuuncellen, samen met de hiteschok-eiwitten HSP70 en HSP90. Bovendien verbeterde NTP-therapie de afgifte van zowel de vroege ICD-marker ATP als de late factor HMGB1. Ter evaluatie van de immuuncel functie toonden DC co-cultuurexperimenten een verhoogde HNSCC tumorcel fagocytose na NTP-CIS combinatie, duidend op een betere immuunherkenning. Deze resultaten benadrukken het potentieel van NTP om de behandelingswerkzaamheid en de tumor immunogeniciteit te verbeteren, vooral in combinatorische setting met standaard middelen. Tot slot bevestigden de organoïden overlevingsdata een hogere tumordoding na NTP-CIS. Samengevat doelde dit project op meer inzicht in HNSCC immunogeniciteit na NTP-CIS combinatietherapie. Zo toonden we aan dat deze veelbelovende toepassing het voorste deel van de kanker-immuuncyclus ondersteunde via ICD-geïnduceerde DAMP-vrijgave. Door verhoging in immunogeniciteit kan de achterkant van de cyclus worden bevorderd en vervolgens resulteren in een systemische en langdurige immuunrespons. Vandaar zullen onze resultaten mogelijks de klinische vertaling versnellen en een cruciale stap zijn richting een rationeel ontworpen combinatiestrategie met NTP om de huidige eerstelijns HNSCC-therapieën te verbeteren.

5 Introduction

5.1 Head and Neck Squamous Cell Carcinoma

5.1.1 Introduction to the Disease

Accounting for nearly 1 in 6 deaths, cancer remains one of the leading public health problems worldwide^[1]. Despite considerable improvements in diagnostic approaches, conventional treatments (e.g., chemotherapy), and new therapeutic modalities that have emerged (e.g., immunotherapy, targeted therapy), additional research is needed to unravel the heterogeneous malignant landscape and circumvent therapeutic limitations^[2, 3].

Head and neck cancer is a hard-to-treat cancer type, responsible for an average incidence of more than 900,000 cases and 400,000 deaths annually^[4, 5]. By 2025, it is estimated that approximately 1,400,000 new patients will be diagnosed with this cancer worldwide and this number is expected to rise even more over the next decade^[6, 7].

More than 90% of these malignancies are **head and neck squamous cell carcinomas (HNSCCs)**, making it the 6th most common cancer type worldwide^[4-6]. HNSCC is a very heterogeneous disease that arises in different anatomical regions of the upper aerodigestive tract, including oral cavity, larynx, and pharynx (Figure 1)^[8-10]. The lining of this tract by the mucosal epithelium with squamous cells has a protective function for the underlying structures. However neoplasia commonly develops here^[11], and interruption of this barrier may provoke cancer invasion and metastasis^[12]. Symptoms of HNSCC are associated with tumor localization: (1) oral cavity tumors are linked to pain when swallowing and chewing^[13], and chronic ulcerations and swelling^[14], (2) laryngeal tumors are typically recognized by hoarseness, as well as dysphagia, otalgia, and a sore throat^[15], and (3) pharyngeal tumors, often as a branch of oropharyngeal squamous cell carcinoma (OPSCC), cover similar symptoms^[16]. Clinical manifestation will eventually interfere with fundamental functions^[14, 15].

The etiology of HNSCC is multi-factorial and diverse among patients, with tobacco smoking and alcohol consumption as the main risk factors. These are primarily linked to malignant development in the oral cavity and pharyngeal subsites due to direct exposure^[17]. As the access to these products is correlated to socio-economic conditions, tumoral burden may vary across countries/regions^[9]. Additionally, HNSCC is most commonly seen in men with an increasing incidence by age, since these lifestyle factors are more predominantly used by males^[18]. Another risk factor is prior viral infection with the human papillomavirus (HPV). HNSCC by this orally transmitted virus will mostly arise in the oropharynx, especially due to high-risk HPV type 16, and to a lesser extent, type 18^[9, 19-21]. The majority of HPV-positive patients are burdened in underdeveloped countries^[22], however, rising incidence has been reported in developed countries and at younger ages^[23]. Interestingly, an HPV-positive status is a positive prognostic factor, since paired immune infiltration is associated with improved survival. By contrast, their HPV-negative counterparts represent worse clinical outcome^[24, 25]. Due to their hard-to-treat nature, this thesis will focus on HPV-negative HNSCC. Besides the major risk factors, other overshadowed contributors are high-fat and processed food^[26], poor oral hygiene^[27], female hormones^[28], physical inactivity^[29], and genetics^[30]. **Despite primary prevention by reducing tobacco and/or alcohol abuse and HPV vaccination, HNSCC still manifests in a growing number of people^[31].**

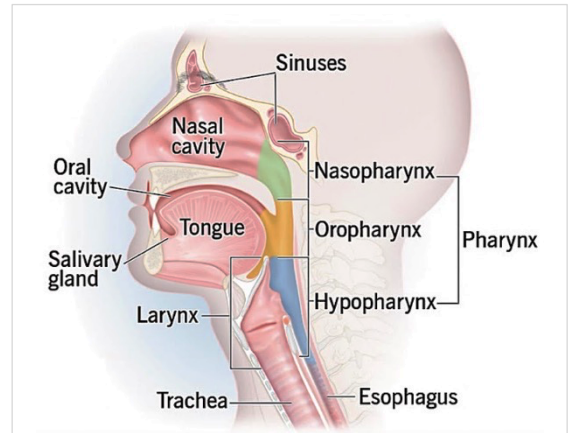


Figure 1. The anatomical sites of head and neck squamous cell carcinoma (HNSCC) development. HNSCC arises from the mucosal epithelium from different anatomical subsites including structures of the oral cavity, pharynx (nasopharynx, oropharynx, and hypopharynx), and larynx^[10].

5.1.2 Drawbacks of Current Standard Treatment Strategies

Both subtype and disease stage are considered as a guide in treatment approach^[32]. The earlier the diagnosis, the better the prognosis and outcome of the disease are^[33]. Conventional therapeutic strategies for early stage patients (stage I and II) include primary surgery or radiotherapy, in a curative setting. Localized early stages are 30-40% of all HNSCC cases and typically have a favorable 5-year overall survival of 90%, with hardly any treatment difficulty^[34]. Unfortunately, most patients (almost 2 out of 3) are diagnosed in the advanced disease stages (stage III and IV), exhibiting an extremely complex pathology with significant therapy- and patient-related unmet needs^[35, 36].

These stages encompass major treatment challenges and often require a multimodal approach, including combined surgery, chemotherapy, and/or radiotherapy (EXTREME regimen)^[36, 37]. Moreover, patients suffer from postoperative complications, high radiation, and systematic side effects^[38, 39], and are often accompanied by development of treatment resistance^[40]. These shortcomings result in tumor recurrence and/or distant metastasis in **approximately 50% of all patients, known as the recurrent or metastatic (R/M) HNSCC population**^[40, 41]. **In this R/M setting, patients face a dismal prognosis** (6-15 months median survival), with a median 5-year survival rate of 30%^[34, 35], which demonstrates the inadequacy of current treatment options.

Platinum-based chemotherapies, i.e., cisplatin (CIS) or carboplatin, are implemented as standard of care for multiple cancer types, including for R/M HNSCC^[42]. This systemic therapy interferes with DNA repair mechanisms by crosslinking to DNA-purine bases, causing cell cycle arrest, and resulting in cancer cell death^[43]. Besides chemotherapy, immunotherapy has been exploited in R/M HNSCC, predominantly the immune checkpoint inhibitors (ICI) pembrolizumab or nivolumab^[44]. The phase III KEYNOTE-048 study showed significantly improved overall survival and longer duration of response versus the EXTREME regimen by combining pembrolizumab and platinum-based chemotherapy, thus supporting the switch to a new first-line treatment strategy in R/M HNSCC setting^[44, 45]. **Despite approval for first-line therapy in the R/M HNSCC setting, treatment is inseparable from considerable limitations:** platinum-based chemotherapies cause severe side effects due to a lack of selectivity (e.g., nephrotoxicity, neurotoxicity, and myelosuppression)^[46, 47], while immune-related adverse events are seen for ICI (e.g., skin toxicities, hepatotoxicity, and pneumonitis), which are considerable risks and challenges for already weakened patients^[48].

As a third drawback, **a very limited patient window is reported (~20%)**^[49]. Low response rates to ICI are assumed to be correlated with downregulation of tumor-expressed programmed cell death ligand 1 (PD-L1), resulting in immunosurveillance escape and even immunotherapy impairment^[50]. As a response to this phenomenon, patient stratification is performed in an attempt to treat patients who are believed to benefit from immunotherapy. This is determined by the patient-specific combined positive score (CPS) for PD-L1, meaning the amount of PD-L1 positive cancer cells relative to the total number of viable tumor cells. According to this score, treatment eligibility is determined: (1) single-agent ICI for patients with CPS $\geq 20\%$ and (2) ICI with platinum-based chemotherapy for patients with CPS ≥ 1 and $< 20\%$. Although high CPS (CPS $> 20\%$) has been positively associated with improved overall survival, few patients benefit due to the consideration of balance between therapy need and concomitant tolerance^[36]. Therefore, research relevance must shift towards the establishment of an increasing number of responders. Taken this together, there is still a major need to overcome limitations of current standard of care modalities, along with improving prognosis and quality of life in R/M HNSCC patients. Hence, development of new treatment options and rationally-designed combination strategies are of utmost importance.

5.2 The Cancer-Immunity Cycle and Immunogenic Cell Death

5.2.1 The Cancer-Immunity Cycle as Therapeutic Target

The human immune system is primarily functioning as the host's protective barrier against a wide range of exogenous invaders^[51]. Although cancer arises endogenously, malignant transformations are generally considered as "non-self" and eliminated by the immune system^[52]. In this way, the human immune system has

a built-in anti-cancer mechanism, called ‘the cancer-immunity cycle’, representing a series of sequential steps that needs to be passed and amplified to elicit a proper anti-tumoral response. This intrinsic immune surveillance is initiated by the release of antigens (Ag) from dying cancer cells. Cancer Ags must be phagocytosed by antigen-presenting cells (APCs), mainly dendritic cells (DCs). These immune cells (cluster of differentiation (CD14+)) are still naïve before contact with the foreign material, so called immature DCs (iDCs). After Ag engulfment and processing, DCs will undergo a maturational reprogramming process to mature DCs (mDCs). Herein, surface-expressed major histocompatibility complex (MHC) molecules are upregulated, enabling Ag surface-presentation. In addition, several co-stimulatory molecules (e.g., CD80, CD83, and CD86) with a designated role in orchestrating T cell-mediated immune responses are expressed: elevated levels of CD80/CD86 provide co-stimulation in T cell activation, whereas CD83 expression is especially important in DC activation. Subsequently, specific interactions between the Ag-loaded MHC molecule and the T cell receptor (TCR), and CD80/86 and CD28, on DCs and T cells respectively, will ensure the transmission of Ag-related information. Due to this interplay, the adaptive immunity will be triggered via priming and activation of the T cells in the lymph nodes. Following this specific activation, effector T cells will traffic to the tumor site and infiltrate. After recognition of the cancer Ags on the tumor, cancer cells will be killed specifically and release novel tumor Ags, triggering an ongoing and durable cyclical process (Figure 2A)^[53-56].

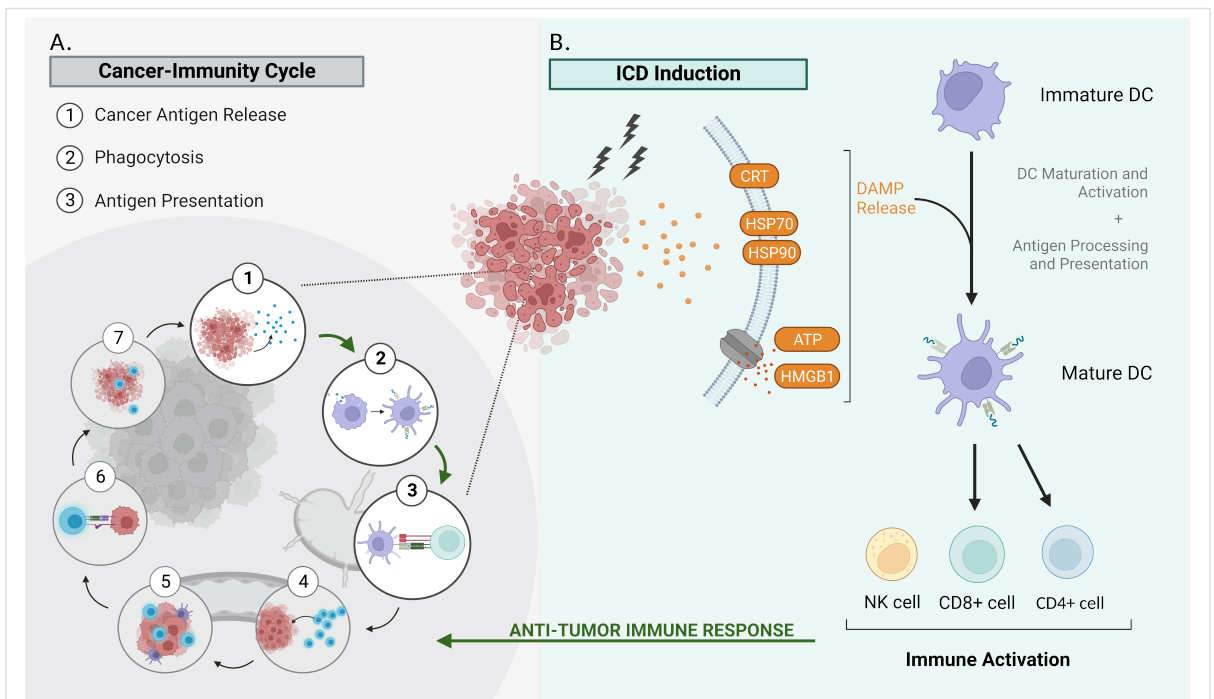


Figure 2. The proposed mechanism during immunogenic cell death (ICD) linked with the cancer-immunity cycle. A) The sequential steps of the cancer-immunity cycle to eliminate tumoral material. B) Established damage-associated molecular pattern (DAMP) release by ICD inducers triggers the intrinsic immune system to mount an anti-tumor immune response. In this way, the front-end of the cancer-immunity cycle will be boosted (indicated with the green arrows) and further amplification of the back-end will enhance tumor eradication. Figure was created using Biorender.

Nevertheless, the biological capabilities cells acquire throughout malignant development, referred to as the **hallmarks of cancer (e.g., metabolic reprogramming and cell death avoidance)**, include the ability of cancer cells to evade the immune system, which undermine this cancer-immunity cycle, eventually leading to immune surveillance failure and malignant progression^[57-59]. At the front-end of the cycle, Ag are deemed to be “self” material and thus escape APCs, which interrupts the following cancer-eliminating steps^[60].

In addition, the tumoral site holds immunosuppressive features such as (1) cell-surface proteins on cancer cells (e.g., downregulation of the MHC)^[61], (2) secreted cytokines (e.g., transforming growth factor beta (TGF- β))^[62] and (3) reprogrammed metabolic pathways (e.g., hypoxia)^[63]. Due to the creation of this hostile space,

impairment in T cell priming and further effector T cell activation is also weakening the back-end of the cancer-immunity cycle^[64, 65].

Hence, cycle restoration appears to be a promising therapeutic strategy to reinitiate the patient's intrinsic immune system and elicit a systemic and durable anti-tumoral response^[54]. Therefore, (re)training the natural defenses by immune-stimulating modalities encompasses a valuable treatment strategy. 2 examples of this immunization strategy in oncology are the DC-based vaccinations, loaded with cancer Ags to mount an attack directed against the tumor^[66], and T cell vaccination, wherein primed T cells encourage a tumor-targeted effector response and long-lasting memory^[67]. Increasing tumor immunogenicity via therapy-induced immunogenic cell death (ICD), stimulating the front-end part, is another research strategy of great interest^[68].

5.2.2 Immunogenic Cell Death Induction as Promotor of the Cancer-Immunity Cycle

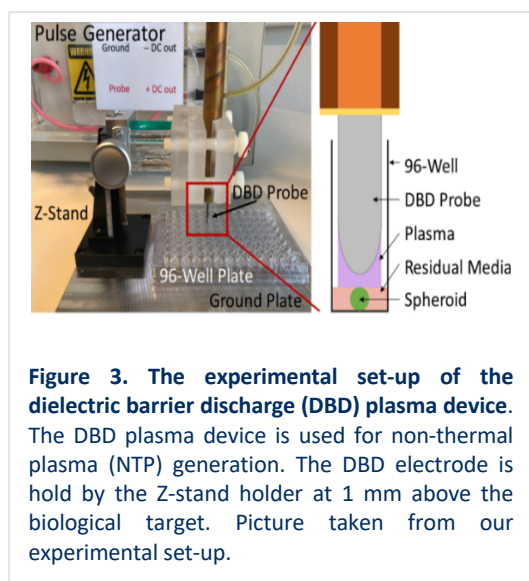
ICD is a form of regulated cell death wherein “danger signals”, called damage-associated molecular patterns (DAMPs), are spatiotemporally emitted to the tumor surroundings by dying tumor cells^[68, 69]. These immunostimulatory DAMPs are recognized by the pattern recognition receptors (PRR) present on iDCs and activate their translation into their mature phenotype, mDCs^[70]. Seen as a stimulatory aid, DAMPs will enhance Ag phagocytosis by DCs, and thereby processed and presented Ags will further trigger the effector cells of the adaptive immunity (CD8+ T cells and CD4+ T-helper cells). In parallel, the innate immunity (natural killer (NK) cells) will be engaged. This patient-intrinsic immune reaction will elicit a specific anti-tumor response (Figure 2B)^[51, 71].

Regarding the cancer-immunity cycle, ICD of tumor cells can initiate different steps, including enhanced Ag release, uptake and phagocytosis. This strong stimulation of the front-end part of the cycle elevates tumor immunogenicity and attracts more effector immune cells, resulting in cancer-immunity cycle amplification and tumor eradication^[72]. Multiple DAMPs have been identified, during this thesis focused on membrane-presented calreticulin (CRT) and heat shock protein (HSP) 70 and 90; and supernatant-released adenosine triphosphate (ATP) and high mobility group box 1 (HMGB1). CRT will translocate from the endoplasmic reticulum (ER) to the surface of the plasma membrane of dying cells^[73]. This occurs at an early stage of ICD, even before membrane disruption^[74]. Exposure of CRT will function as an “eat-me” signal to enhance phagocytosis by DCs^[75]. Molecular chaperones HSP70 and HSP90 are intrinsically important in cellular homeostasis by assisting in protein folding and remodeling^[76]. Regarding dying cells, they are also presented on the cell-surface, which contributes to higher DC maturation^[77]. In addition to these surface-expressed ICD markers, supernatant-released factors are often parallelly examined. The metabolite ATP, a key player in healthy cellular processes, is liberated into the extracellular space by dying cells. Stated as a “find-me” signal, it enables the recruitment of DCs and it mediates pro-inflammatory effects^[78, 79]. Lastly, the nucleus-resident HMGB1 is also released into the cytoplasm, established by permeabilization of the nuclear lamina and plasma membrane^[80]. This marker will be exposed in a later stage of cell death and will eventually interact with the Toll-like receptor 4 (TLR4) as “find-me” signal to engage the DCs^[78, 81].

Several anti-cancer therapies, predominantly chemotherapy and radiotherapy, have been reported to have the ability to induce ICD, thereby enhancing tumor immunogenicity^[82, 83]. Immunogenic changes after monotherapy or combined application of platinum-based chemotherapy and radiotherapy have been demonstrated by increased levels of CRT, HSP70, and HMGB1^[82, 84]. Interestingly, chemotherapeutics like HNSCC first-line CIS have been appointed to induce ICD, majorly when administered in a specific concentration range, lower than given in the past^[84]. Although the underlying mechanism of action of ICD induction is still under extensive investigation, it is assumed to be correlated with treatment-mediated ER stress and reactive oxygen species (ROS) production^[70, 74], making it an interesting therapeutic target. It has been stated that ICD expression implies clinical relevance by enhancement of immunogenicity^[78]. Wang et al. reported the correlation between overexpressed ICD markers and improved overall survival in HNSCC, indicating the possible use of ICD markers as prognostic signatures^[85]. Furthermore, ongoing clinical trials are evaluating the benefits of ICD prediction for different tumor types, including lung, breast, and ovarian cancer^[86]. For these appealing properties, several emerging ICD inducers are being investigated in-depth for its potential as cancer therapy. One such novel modalities is non-thermal plasma (NTP), plasma generated at room temperature and atmospheric pressure^[87, 88].

5.3 Non-Thermal Plasma

5.3.1 The Anti-Cancer Activity of Non-Thermal Plasma



NTP is an emerging anti-cancer strategy currently being investigated^[71]. Plasma, a state of matter, is formed by gas ionization. In contrast to high temperature ‘thermal plasma’, NTP for medical applications is generated at room temperature and atmospheric pressure. It consists of a complex mixture of reactive oxygen and nitrogen species (RONS), charged particles, and ultraviolet light^[88-90]. 2 different approaches to create NTP are widely used in plasma medicine: the plasma jet device and the dielectric barrier discharge (DBD) plasma device (employed during this thesis)^[89]. For the plasma jet, plasma is generated in the device and delivered to the biological target by a carrier gas^[91, 92]. In contrast, DBD plasma is directly generated between the high voltage copper electrode and the target cells or tissue (Figure 3)^[93]. Treatment conditions (e.g., treatment time, application distance), and device characteristics (e.g., pulse duration, electric field intensity) are adjustable^[93].

NTP has been shown to be effective for inducing anti-cancer activity, both *in vitro* and *in vivo*. *In vitro*, the effect of NTP on multiple cancer cell lines have been investigated, including HNSCC^[89, 94, 95]. In addition, *in vivo* studies of NTP, using different mouse models, have demonstrated recruitment of immune cells, reduction in tumor burden, and improved animal survival^[88, 96, 97]. Even more, the first clinical trial using NTP has been established by Metelmann et al. for locally advanced OPSCC patients. They reported both improved quality of life and partial tumor remission in some patients^[98].

The molecular working mechanism of NTP is extensively investigated, with a special focus on ER stress and the intracellular redox balance^[99, 100]. This redox state is essential to maintain, since low/moderate levels are fulfilling a crucial role in cellular metabolism and physiological processes, resulting in maintained homeostasis^[101, 102]. Unlike balanced generation and elimination in healthy circumstances, excessive ROS production, inducing ER stress, will deteriorate the cellular cytoskeleton, proteins, and genetic material leading to cell cycle arrest or cell death^[103, 104]. As malignant transformation is characterized by metabolic reprogramming, elevated rates will result in higher basal levels of ROS in cancer cells^[105]. Therefore, it is stated that malignant cells may be more susceptible to oxidative stress, by exceeding the harmful ROS threshold, resulting in a selective treatment window^[100].

A further subdivision of the RONS can be made in short-lived (lifetime < 1sec: •OH, •NO, O/O₃) and persistent (lifetime > 1sec: ONOO⁻, H₂O₂, NO₂⁻, NO₃⁻) species^[87]. Intriguingly, having extensive experience in this topic, our lab was the first to report the specific short-lived RONS as the major contributor to ICD induction, confirming NTP as an emerging ICD inducer and thereby underlining its potential as an immune-stimulating anti-cancer therapy^[87, 88]. Based on these appealing characteristics, **NTP could be a valuable addition to current treatment strategies^[71].** NTP in combination with chemotherapy^[106], radiotherapy^[97], and targeted therapy^[107] is reported to have inhibitory effects on cancer cell proliferation and invasiveness in different cancer types, including HNSCC^[107]. In that light, the focus of this thesis is to explore the effect of NTP in combination with first-line chemotherapy for R/M HNSCC^[99].

Since current R/M HNSCC first-line ICI treatment with or without chemotherapy has considerable shortcomings (i.e., severe side effects^[46, 47] and select response rates^[49]), NTP holds great potential to circumvent these limitations by its capacity to induce ICD. Moreover, **no major side effects have been reported yet regarding clinical application of NTP**, which is a very appealing property for already weakened patients and potentially a critical advantage over other therapies^[71, 108]. Taken together, due to reported benefits and attractive properties of combination strategies, we aim to elucidate the possible amplified effect of conventional CIS chemotherapy with emerging NTP treatment in HNSCC.

5.4 3D Tumor Models to Better Mirror the Tumor Microenvironment

5.4.1 The Limitations of 2D Cell Cultures

In vitro cell cultures are valuable research models in diverse fields, including cancer research, to assess characteristics related to cell biology, tissue morphology, and disease mechanisms. They have been irreplaceable in the development of new treatment modalities and in studying treatment resistance^[109, 110].

In two-dimensional (2D) cell culturing, cells adhere on a flat plastic surface, growing into a uniform monolayer, thereby equally accessing the nutrient-containing medium. By sub-culturing, confluence is delayed allowing maintained cell growth^[111]. 2D cultures are routinely used since they are simple, fast, low-cost, highly reproducible, and compliant to high-throughput screening^[112]. Although this culturing method is widely applied in cancer research to understand fundamental malignant characteristics, **consensus is emerging that flat monolayers lack the ability to reflect essential components of the complex tumoral context – the tumor microenvironment (TME)**^[109, 110, 113, 114]. Other limitations are cell polarization, loss of heterogeneity, and altered cellular homeostasis and functioning (e.g., migration and signaling processes)^[110, 115]. These shortcomings impair *in vivo* translation and clinical implementation, as evidenced by the low development rate of successful treatment strategies^[116].

5.4.2 The Appearance of the Complex Tumoral Setting

Besides cancerous cells, the tumoral context consists of a multidimensional extracellular matrix (ECM) and diverse cell populations, altogether considered as the TME^[113], seen as **structural and functional elements with a pleiotropic character to support malignant development**^[117].

In addition to the physical support, the ECM plays a major role in modulating cellular behavior^[118]. The composition is found to influence cell characteristics contributing to cancer cell proliferation, dissemination and, tumor-promoting cell signaling^[119]. Another major determinant is the concentration gradient, seen as non-uniform multidimensional zones, going from a necrotic core of cell death to viable and proliferating tumor cells in the outside layers. This way, there is a gradient of restricted diffusion of oxygen and nutrients, with a built-up of CO₂ and metabolic waste products in the center (e.g., lactate). As seen in an *in vivo* or clinical setting, drug distribution to the tumoral center is physically restricted, causing an inhomogeneous treatment delivery throughout the tumor^[120, 121]. Due to the absence of the multidimensional structure in a flat, monolayer culture, this aspect is not implemented in 2D cultures. Therefore, it has been stated that a higher inhibitory concentration 50% (IC₅₀) dose is needed in three-dimensional (3D) models to obtain the same results as 2D cultures, encompassing a better reflection and relevance regarding further human translation^[121, 122]. Alongside the ECM, the tumoral setting is populated by diverse cell types such as cancer-associated fibroblasts (CAFs), neuroendocrine cells, immune cells, and adipocytes^[117]. These tumor-supporting cells are linked with malignant progression, low drug effectiveness and poor clinical outcome^[123, 124].

Hence, implementation of these cell-cell, and cell-ECM interactions are thus of utmost importance to mirror tumor mass architecture and functioning^[114], and underline the lack of 2D cultures to be representative. Therefore, a next generation of models that implement these features to mimic the tumoral site is needed in oncological research, to advance novel treatment development and clinical translation.

5.4.3 The Current and Future Successes of 3D Cell Cultures

The last decade, research has been shifted to more advanced culturing perspectives to better display the complex malignant environment, namely 3D cell cultures^[125]. **3D models are able to respond to several 2D model shortcomings, including ECM scaffolding, a diffusion (nutritional) gradient, and multidimensional intercellular interactions**^[120, 126].

An established method, implemented in this thesis, is the 3D spheroid tumor model. These are multi-aggregates of tumor cells that obtained their spheroidal shape via matrix support and non-adherent seeding^[127]. Since they

include aforementioned 3D model enhancements, they have showed to be a more representative tool in oncological research and drug assessment^[128]. Regarding HNSCC spheroids, they have demonstrated to better mimic clinical drug responses due to nonhomogeneous distribution of drug concentrations, and often partial treatment response throughout the spheroid^[129]. Also, applied in this thesis, they have showed to be feasible for studying programmed cell death^[130], including ICD induction and immunogenicity^[131, 132]. By these studies, conceptual evidence will eventually result in a better clinical translation^[130].

However, as they are derived from cell lines, tumor spheroids exhibit restricted heterogeneity due to the progression of only one cellular subtype^[110]. To respond to this, co-cultures with other cell types (e.g., immune cells, fibroblasts, endothelial cells) are suggested. Last decade, considerable research into co-culturing immune cells with various cancer types, including colorectal cancer^[133], breast cancer^[134], and even HNSCC^[135], revealed tumor-immune interactions and therapeutic potential, thus highlighting the importance of the immune system crosstalk. In that regard, during this thesis, co-culturing with monocyte-derived DCs, isolated from peripheral blood mononuclear cells (PBMCs) of donor buffy coats, will be evaluated to assess activation of the immune system and improvement in spheroid tumor killing.

Besides the spheroid model, more complex and advanced 3D approaches exist, including the patient-derived organoid model (PDO). This 3D tumor model originates directly from patient tissue, thereby optimally recapitulating the patient's tumor characteristics and heterogeneity in varying cell types. Besides copying the phenotypic landscape, the mutation and expression profile of the patient's tumor are adopted. Since it is considered as a 'patient-in-the-lab', organoids hold great promise for drug screening and personalized medicine applications^[136]. Recently, it has become apparent that they are feasible to predict the *in vivo* drug response of the patient, confirming great potential to be implemented in the treatment decision-making process^[137].

Taken together, 3D models can better mimic both physiological and pharmacologic tumor characteristics and are thereby better in mirroring the *in vivo* and clinical situation. During this thesis, the 3D spheroid tumor model will be used for ICD assessment experiments and the PDO model will provide the validation of results.

6 Aims and Objectives

Current HNSCC first-line treatment (chemotherapy and immunotherapy) is limited by several drawbacks, including severe side effects and low response rates. The novel, emerging therapy NTP has already showed preclinical anti-cancer efficacy and feasibility in the clinic, without reports of major side effects. In addition, NTP holds great potential as an ICD inducer, mainly via the delivery of short-lived RONS ($\bullet\text{OH}$, $\bullet\text{NO}$, O/O_3), which trigger several cellular stress mechanisms. Contrary to previous literature, HNSCC first-line chemotherapy CIS is now also reported to induce features of ICD, specifically in low-dose regimens, which can be further amplified with other ER stressors. Taken together, we hypothesized that NTP could be a well-tolerated ER stressor with first-line CIS treatment in HNSCC to increase tumor immunogenicity and treatment response, while limiting adverse effects. By boosting the front-end of the cancer-immunity cycle, the back-end part can indirectly be amplified to subsequently improve systemic and long-term anti-cancer immunity in HNSCC patients.

Therefore, the aim of this study is to evaluate the immunogenicity of HNSCC tumor cell death after NTP-CIS combination therapy, through the assessment of ICD induction via DAMP release and immunological functionality via DC co-culture experiments. Besides this, we aimed to preliminary validate our NTP-CIS combination therapy. All experiments will be performed using a DBD plasma device. To obtain this goal, 3 objectives have been stated:

1) Characterization and quantification of DAMPs following combination treatment of NTP-CIS. 3D spheroids, made from 3 different HNSCC cell lines, will be exposed to different treatment regimens of CIS concentrations and/or NTP intensities, predefined in our lab. To assess ICD induction, a panel of various DAMPs will be evaluated at fixed timepoints. Membrane-expressed markers, including CRT, HSP70, and HSP90, will be examined with immunofluorescent staining and microscopy. Supernatant-released markers, including ATP and HMGB1, will be evaluated using the ENLITEN[®] ATP assay and the HMGB1 express ELISA, respectively.

2) Evaluation of DC activation/maturation, and phagocytosis of cancerous cells in co-culture experiments. CD14⁺ monocytes, isolated from donor-derived buffy coats, will be differentiated to iDCs, which will be subsequently added to NTP-CIS pre-treated HNSCC spheroids. The co-culture will be maintained for 48h, in order for iDCs to recognize and engulf the tumor cells, leading to immune activation. The maturation process towards a mDC phenotype and phagocytosis events will be examined with flow cytometry analysis.

3) Validation of immune activation after double treatment (NTP-CIS) in HNSCC organoids. Patient-derived organoids of HNSCC will be treated with previously optimized CIS concentrations and/or predetermined NTP intensities. Brightfield and fluorescent live-cell imaging with a cell death marker will be performed via continuous 4h scans to evaluate tumor kinetics and organoid cell death.

7 Materials and Methods

7.1 Cell Cultures

A panel of 3 different human HNSCC cell lines was used, namely Cal27, SCC22B and SCC61. Cells were cultured in Dulbecco's Modified Eagle Medium (DMEM) supplemented with L-glutamine (1%), penicillin/streptomycin (1%), and Fetal Bovine Serum (FBS) (10%). The cell lines were maintained as monolayers in cell culture flasks and incubated in a humidified incubator with controlled 37°C and 5% CO₂ conditions. When confluency of 80 to 90% was reached, cells were sub-cultured to retain their exponential growth curve (i.e., log phase) and to restore essential nutrition. Sub-culturing was done by a washing step using PBS, whereafter the cells were detached with trypsin (Life Technologies™). For experimental cell counts, the average live cell number and viability were retrieved from the TC20 automated cell counter (1450102, Bio-Rad®) using trypan blue (Life Technologies™) in a 1:1 ratio. The cell lines were confirmed to be free of mycoplasma infection by regular testing.

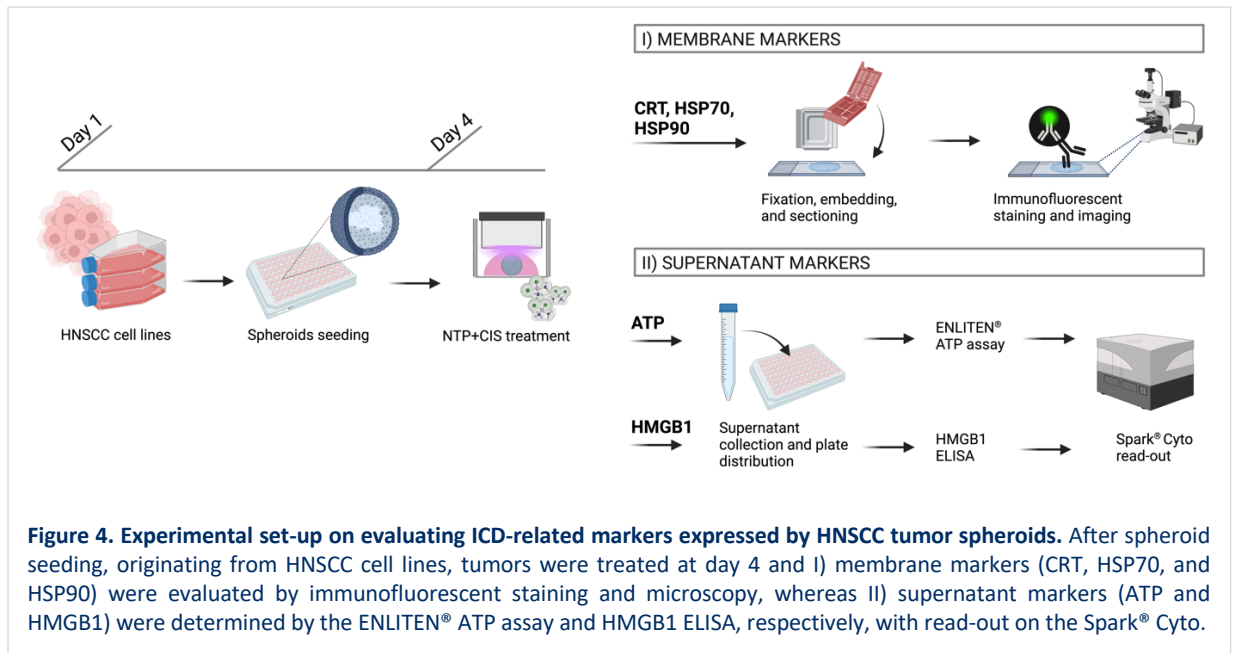
7.2 3D Spheroid Tumor Model

A 3D spheroid tumor model was used by the implementation of a protocol previously optimized in our lab. To promote spheroid formation, by preventing surface attachment, HNSCC cell lines were seeded in coated, round-bottomed 96-well ultra-low attachment (ULA) plates (7007, Corning®). The optimal cell seeding concentration was cell line specific: 4x10⁴ cells/mL for both Cal27 and SCC22B, and 5x10⁴ cells/mL for SCC61 (100 µL/well). The cell suspension was supplemented with 2% Matrigel DB Phenol Red Free (354230, Corning®) to provide additional support for spheroid condensation. After centrifugation (1200 rpm, 10 min, 4°C), the plate was left undisturbed for 3 days of incubation to obtain a spheroid size of 350-450 µm (Figure 4).

7.3 NTP-CIS Double Treatment Strategy

7.3.1 NTP with DBD Device

A microsecond-pulsed dielectric barrier discharge device (mspDBD) was used for NTP application throughout all experiments (Figure 4). The operational characteristics of the device have been previously determined in our lab^[138]: the function generator manages the adjustable parameters of frequency (Hz), treatment seconds (sec) and pulses (cycles), powered by the power supply. The quartz-coated electrode connected to the power supply is placed in a Z-stand holder. A calibrated distance of 1 mm was maintained between the electrode and the biological target. For treatment, spheroids were picked up from the curved 96-well plate, transferred to a flat 24-well plate, and treated with NTP at a frequency of 1000 Hz for 10 sec (10,000 cycles). After treatment, tumors were transferred back to the ULA plate, immediately covered with 200 µL fresh medium, and incubated under controlled conditions until further experimental read-outs. For PDO validation, organoids could be directly treated in the flat, coated 96-well plate.



7.3.2 Cisplatin Treatment

Cisplatin (S1166, Selleckchem[®]) administration was performed by the automated D300e Digital Dispenser (399177, Tecan[®]) (Figure 4). The stock concentration of CIS (5mM) was diluted in aqueous medium with Tween-20 (30%) in a 1:1 ratio. The required volumes were added to the application cassette, allowing an automated and controlled delivery to the experimental plate. CIS concentrations have been previously determined in our lab via a 7-point titration. Herein, 2 concentrations were selected: (i) a low CIS concentration (CIS_{low}) showing almost no cell death after 24h, and 25% of cell death 48h after treatment; and (ii) a high CIS concentration (CIS_{high}) exhibiting cell death percentages of 25% at 24h, and 50% at 48h after treatment. These percentages were chosen based on biological relevance and to preserve a treatment window to observe combinatorial effects. Since these values are cell line specific, the CIS working concentrations have been listed as follows: (1) Cal27: CIS_{low} 1.71 μM and CIS_{high} 5.85 μM, (2) SCC22B: CIS_{low} 0.925 μM and CIS_{high} 3.16 μM, and (3) SCC61: CIS_{low} 5.85 μM and CIS_{high} 20 μM.

Accordingly, in the assessment of ICD induction during this thesis, 6 different treatment regimens were included across all experiments (Table 1). Treatment conditions included an untreated control (UT), a low CIS concentration (CIS_{low}), a high CIS concentration (CIS_{high}), plasma monotherapy (NTP), and both combinations of NTP with respective CIS concentration (NTP-CIS_{low} and NTP-CIS_{high}). At the end of the treatment, each plate yielded 5 spheroids per condition per timepoint.

Table 1. The treatment plate map used throughout all experiments according to 6 conditions. This scheme of a 96-well plate was used across all experiments, resulting in 5 spheroids per condition per timepoint. Cell line specific CIS concentrations were previously determined at our lab. NTP treatment was performed at 1000 Hz with a fixed treatment time of 10 sec.

	1	2	3	4	5	6	7	8	9	10	11	12
A		Timepoint 1					Timepoint 2					
B	UT	[Black shaded cells]										
C	CIS _{low}	[Green shaded cells]										
D	CIS _{high}	[Orange shaded cells]										
E	NTP	[Teal shaded cells]										
F	NTP-CIS _{low}	[Orange and green striped cells]										
G	NTP-CIS _{high}	[Green and orange striped cells]										
H		[Empty cells]										

7.4 Agarose Embedding and Preparation of Microscopic Slides

For evaluation of the expression of membrane-associated ICD markers after NTP-CIS combination therapy, spheroids were fixated 24h hours after treatment in 4% paraformaldehyde (PFA) (100 μ L). After incubation (1h, RT), spheroids were transferred to agarose molds for further processing. In short, 2 mL of hot (50-70°C) agarose solution (4% w/v in deionized water) was dispensed in pre-warmed (37-50°C) stainless steel histology molds, followed by making a grid print with the mold-maker (in-house made). When the agarose was fully solidified (2 min at RT, 1 min at -18°C), the mold-maker was gently removed to prevent the gel from breaking. Previously fixated spheroids were transferred to the agarose grid, whereafter 0.5 mL low-melting point agarose (2% w/v) was slowly added to seal the spheroids in the gel (Figure 5). Agarose pads were placed in plastic histology cases, immersed in PFA, and tissue processed; whereafter pads were sectioned for microscopy purposes (Figure 4).

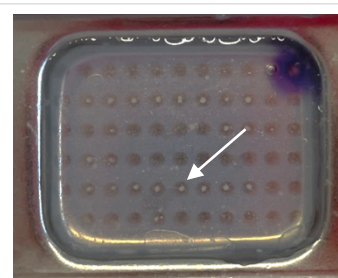


Figure 5. Pre-treated spheroids were transferred individually into the separated agarose pores of the mold (indicated by arrow).

7.5 Immunofluorescence and Imaging

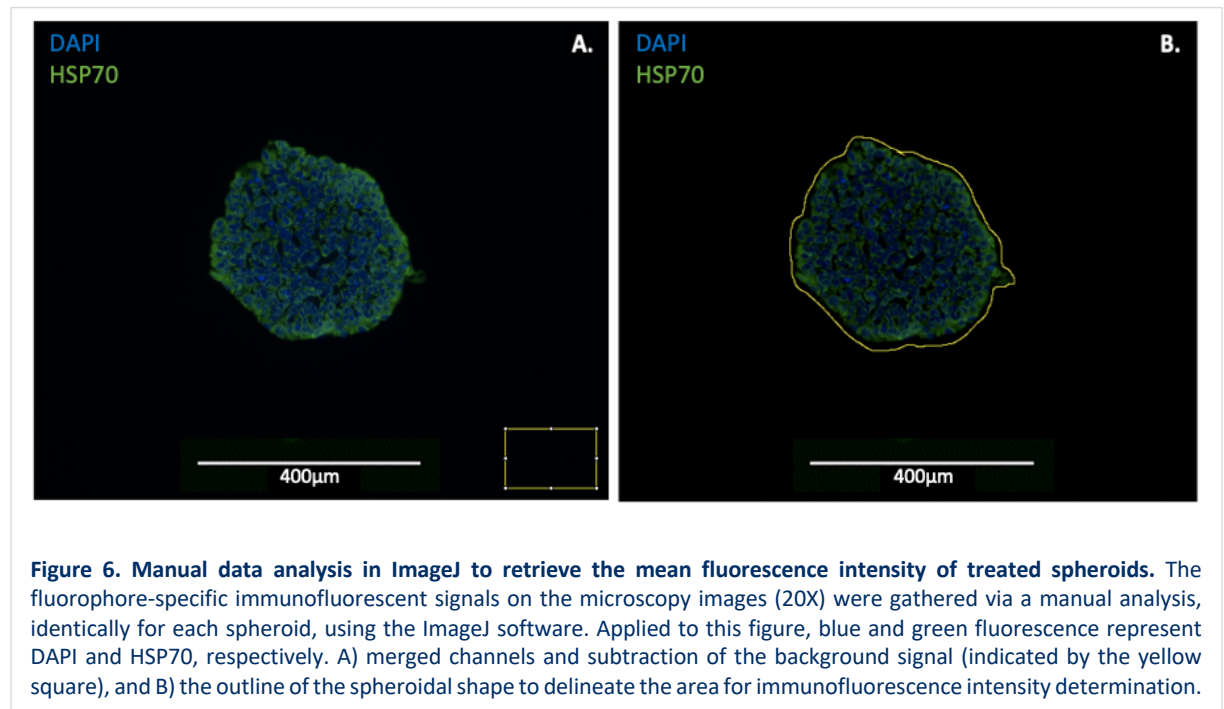
Microscopy slides were baked (2h, 60°C); and washed with xylene (2x, 3 min), decreasing concentrations of isopropanol (100-50%, 1x, 3 min), and H₂O (2x, 5 min) for deparaffinization. From this step, samples were not allowed to dry anymore to avoid non-specific antibody binding. Automated antigen retrieval was performed (DAKO, 97°C, pH6), and slides were washed (2x, 5 min) in tris-buffered saline (TBS) with 0.025% Triton X-100. The immunofluorescent staining antibodies to assess ICD membrane markers, listed in table 2, have been previously titrated by our lab. To prepare staining procedures, the spheroid-containing areas on the slides were delineated using a hydrophobic IHC (PAP) pen. To avoid aspecific binding, blocking was performed with serum (10%), matched with the host species of the secondary antibody. Lastly, the primary antibody was applied, diluted in blocking buffer (1%), and incubated overnight (16h, 4°C).

Table 2. Antibodies for staining of CRT, HSP70 and HSP90 for immunofluorescent imaging. After antigen retrieval, the target will be captured by the primary antibody. The fluorophore-conjugated secondary antibody will bind to the primary antibody and eventually emit fluorescence.

Staining	Primary antibody	Secondary antibody
CRT	Rabbit monoclonal (ERP3924) to Calreticulin (ab92516) 1/500	Goat Anti-Rabbit IgG H&L (Alexa Fluor® 488) (ab150077) 1/1000
HSP70	Rabbit Recombinant Anti-Hsp70 antibody (ab181606) 1/50	Goat Anti-Rabbit IgG H&L (Alexa Fluor® 488) (ab150077) 1/1000
HSP90	Anti-Hsp90 antibody (AC88) (ab13492) 1/200	Donkey Anti-Mouse IgG (H+L) (AlexaFluor 594) 1/500

The next day, samples were washed with TBS 0.025% Triton (2x, 5 min). The fluorophore-conjugated secondary antibody, diluted in 1% blocking buffer, was added to the slides, and incubated (1h, RT). To avoid photobleaching, following steps were conducted in a dark environment. After final washing, slides were mounted with antifade mounting medium with DAPI nuclear counterstain (ab104139, Abcam), followed by gentle covering with a coverslip. Samples were stored in a cold (4°C), dark environment upon imaging.

Image capturing was performed with the Olympus BX51 fluorescence microscope (WSBX51-0169, Olympus Life Sciences) (Figure 4). Fluorescent images were taken (20x magnification), and exposure time was determined per fluorophore, aiming minimal background signal. Applied settings were maintained throughout the entire experiment. The ImageJ software was used to evaluate fluorescence intensities (Figure 6), whereafter the data was analyzed and processed in GraphPad Prism9.



7.6 ATP Secretion

To evaluate secreted ICD factors after NTP-CIS combination therapy, ATP and HMGB1 were evaluated in the supernatant. First, ATP release from the treated spheroids was quantified with the ENLITEN® ATP assay system bioluminescence detection kit for ATP Measurement (FF2000, Promega) (Figure 4). Following the manufacturer's instructions, the assay was performed on freshly collected supernatant. In brief, the reconstituted reagent was prepared freshly by gently merging the reconstitution buffer and ENLITEN® rLuciferin/Luciferase Reagent, followed by one hour of incubation before analysis initiation (1h, RT). Spheroid medium (supplemented with heat inactivated FBS) was collected and pooled by condition at 2 different timepoints, 4h and 24h after treatment.

In parallel, an ATP standard curve was prepared out of a 5-points serial dilution, ranging from the ATP stock concentration (10^{-7} M) until fully diluted standard (10^{-11} M). Each condition/standard was transferred to a white, opaque 96-well plate (6005689, PerkinElmer) and mixed with reconstituted ATP reagent in a 1:1 ratio. After short incubation (5 min, RT, dark), the bioluminescent signal was measured with the Spark® Cyto (Tecan). A blank (medium) control was subtracted from all signals, and the amount moles of ATP was retrieved by the standard curve equation.

7.7 HMGB1 Release

The amount of HMGB1 release of NTP-CIS treated spheroids was quantified in frozen supernatant with the HMGB1 express enzyme linked immune sorbent assay (ELISA) kit (30164033, Tecan) (Figure 4). Experimental steps were performed according to the manufacturer's prescription. In brief, the supernatant of NTP-CIS treated spheroids was collected and pooled per condition at 2 timepoints, 48h and 72h after treatment, and frozen down for later usage and batch-processing (-80°C). A negative (0 ng/mL) and positive (80 ng/mL, pig HMGB1) control

were included. At analysis initiation, 100 μL of a 7-points prediluted standard, controls, and samples were added in a microtiter plate, coated with antibodies against HMGB1. After incubation (2h, 37°C), the plate was washed with 400 μL wash buffer (5x). Hereafter, 100 μL enzyme conjugate was pipetted into each well and further incubated (1h, +25°C). After repeating the washing step (5x), 100 μL of premixed color solution was added. The reaction was punctually interrupted by addition of 100 μL stop solution (20 min, RT, dark). Finally, the optical density was measured at wavelength 450 nm using the Spark[®] Cyto and the HMGB1 levels were retrieved by the standard curve equation. All signals were corrected to the manufacturer's proposed reference wavelength (600-650 nm).

7.8 Co-Culture of HNSCC Spheroids with Monocyte-Derived Dendritic Cells

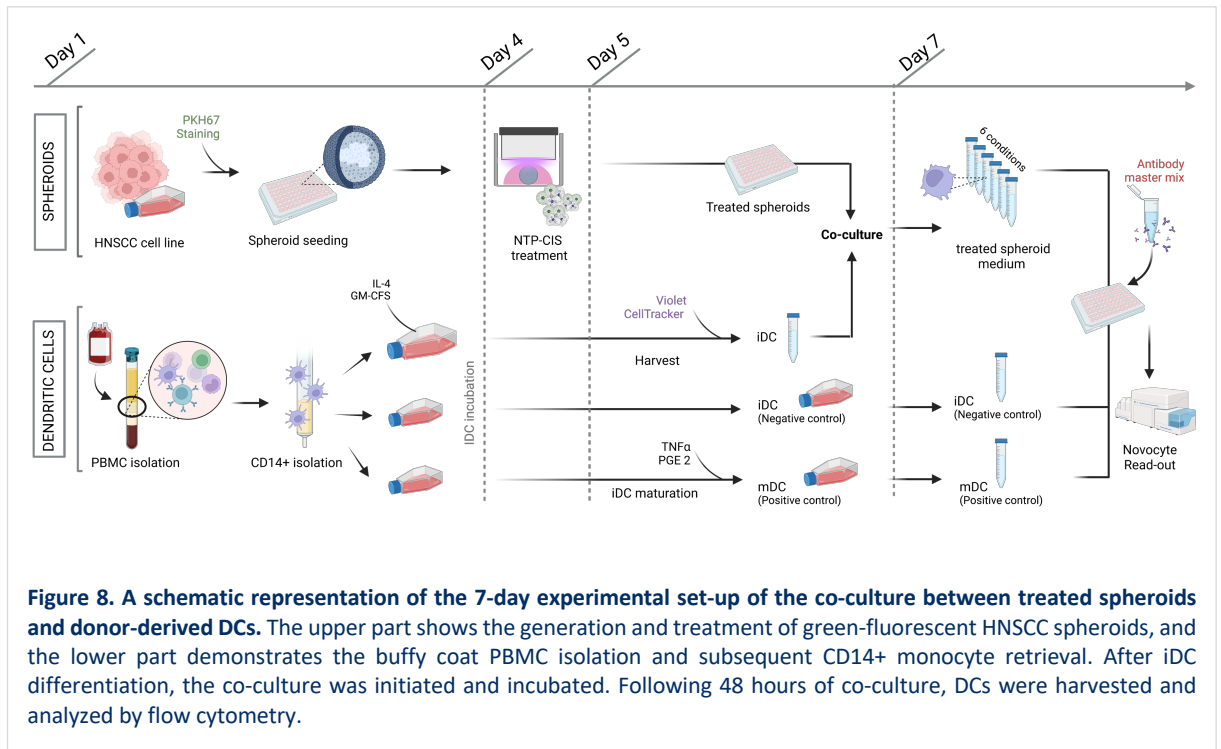
7.8.1 Generation of Monocyte-Derived IDCs and Green-Fluorescent Spheroids (Day 1-4)



Figure 7. The obtained PBMC fraction after Ficoll density-gradient centrifugation of the buffy coat. After centrifugation of a healthy donor's buffy coat, the obtained PBMC fraction became visible as a separated, white ring (indicated by arrow). Next, monocytes were isolated by a positive selection using CD14+ magnetic beads.

Human PBMCs were retrieved of healthy donor's buffy coats, provided by the Red Cross (Flanders). Purification of these cells was established using Ficoll density-gradient centrifugation (Ficoll-paque plus, 17-1440-03, VWR)^[139]. Hereafter, **monocytes were isolated from the PBMC fraction by CD14+ positive selection**, based on magnetic cell sorting (200-070-118, Miltenyi Biotec) (Figure 8). After the PBMC sample had run the LS column (130-042-401, Miltenyi Biotec), the bead-bound CD14+ monocytes were retrieved by firm flushing^[140]. Monocyte purity (95%) and viability were verified by flow cytometric measurement (CytoFLEX, Beckman Coulter). To further generate iDCs, CD14+ monocytes were plated out at day 0 at a density between $1,00 \times 10^6$ and $1,25 \times 10^6$ cells/mL in Roswell Park Memorial Institute (RPMI) 1640 Medium (21875034, Life Technologies[™]), supplemented with 2.5% human AB serum (hAB, Sanbio), 800 IU/mL granulocyte macrophage colony stimulating factor (GM-CSF) (130-095-372, Miltenyi Biotec), and 20 ng/mL interleukin (IL)-4 (130-093-917, Miltenyi Biotec). iDC were retrieved after 5 days of undisturbed incubation (37°C, 5% CO₂).

In order to visualise phagocytosis at day 7, tumor cells underwent intracellular PKH67 staining prior to spheroid seeding. Harvested HNSCC cells were green-fluorescently labelled in unsupplemented medium by addition of 1 μL PKH67 reagent per 1×10^6 cells, diluted in 500 μL Diluent C. After several washing steps (3x), the stained tumor cells, immersed in medium with supplements, were plated out following the standard 3D spheroid tumor model protocol as described above.



7.8.2 DC Co-Culture and Flow Cytometric Analysis of Maturation and Phagocytosis (Day 5-7)

HNSCC spheroids were treated 24h prior to the start of the co-culture (Day 4) according to the treatment scheme above (Table 1).

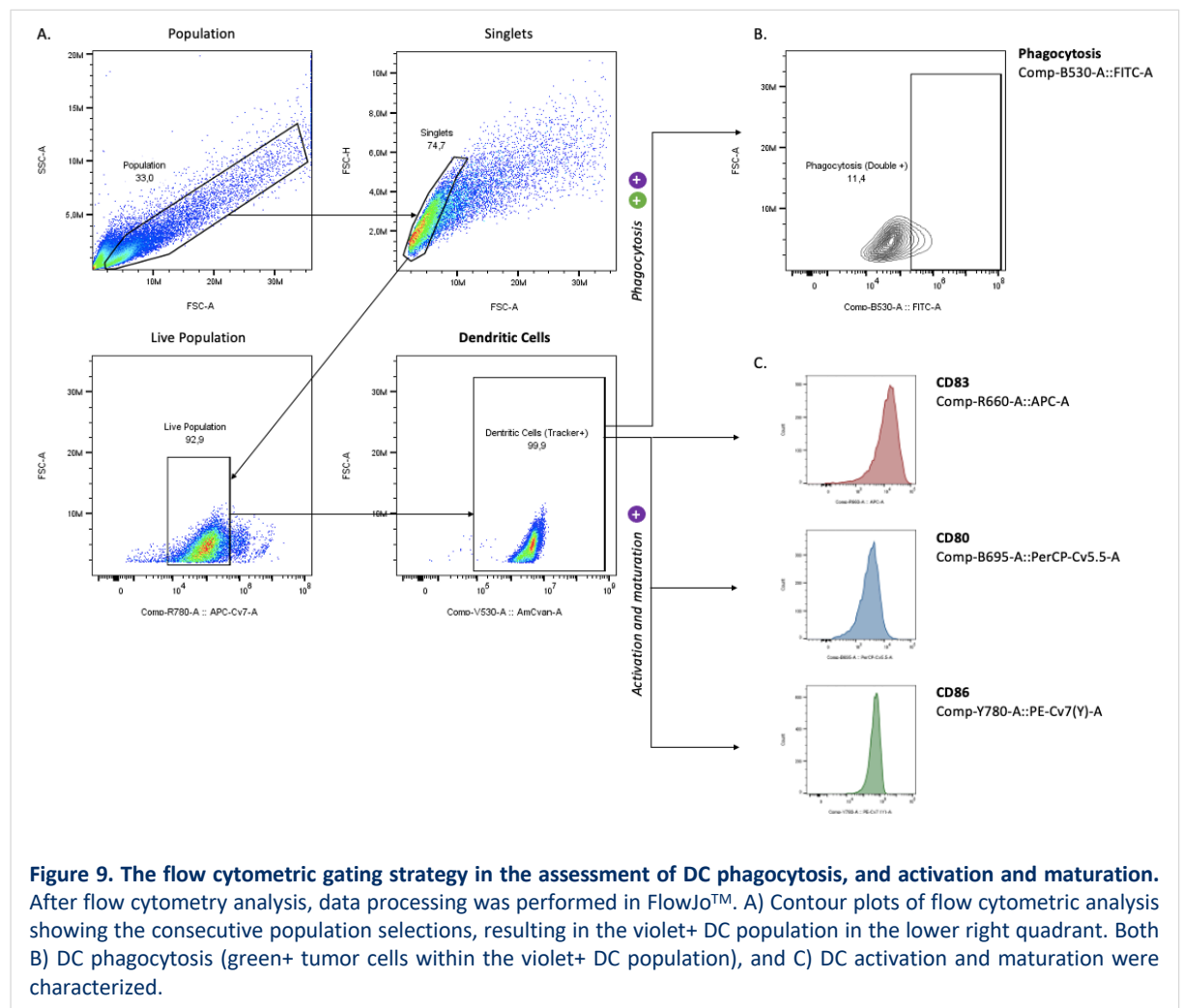
On day 5, iDCs were harvested and cell count was determined, whereafter the cells were labelled with CellTracker™ Violet BMQC dye (C10094, Invitrogen™). In this way, DC (violet+) phagocytosis of tumor cells (PKH67+) was represented as double positives during flow cytometric analysis. Harvested iDCs were resuspended in 1 mL of 2 μM violet tracker per 1x10⁶ iDCs and incubated for 30 min in a warmed environment (37°C). Staining was terminated with resuspension and incubation in full DC medium (30 min, 37°C). iDC suspensions at a concentration of 3x10⁵ cells/mL were prepared and added to the pre-treated spheroids at an 1:1 effector-target (E:T) ratio. Unstimulated iDCs without co-culture were included as negative control. Fully matured DCs (mDC), retrieved from iDCs stimulated with a maturation cocktail of TNF-α (8 μL/mL) and PGE 2 (4 μL/mL) counted as positive control.

After 2 days of co-culture (37°C, 5% CO₂), spheroids were firmly flushed with PBS-EDTA in order to detach all adherent DCs. After spheroid discard, DCs were harvested via medium collection and pooled per condition. After washing with PBS-EDTA and centrifugation (1500 rpm, 5 min, 4°C), DC pellets were resuspended in FACS buffer. In parallel, cell count of the controls was adjusted to the same concentration as the experimental conditions. After centrifugation (1500 rpm, 5 min, 4°C), each pellet was resuspended in 50 μL antibody mix and incubated (30 min, 4°C). The master mix consisted of antibodies against different activation and maturation markers present on mDCs, including anti-CD80-PerCPCv5.5 (400150, Biolegend), anti- CD83-APC (551073, BD Biosciences), and anti-CD86-PE-Cv7 (Y) (557872, BD Biosciences); along with Invitrogen™ LIVE/DEAD Fixable Near IR (876) Cell stain (L34981, Thermo Fisher Scientific). Finally, flow cytometry analysis was performed at the Novocyte Quanteon (Agilent) to assess DC phagocytosis and maturation.

7.8.3 Gating Strategy

In order to assess phagocytosis, and activation and maturation markers, DCs were stained with a violet, fluorescent dye as described above, for the purpose of visualizing interactions with the pre-treated spheroids that were stained green.

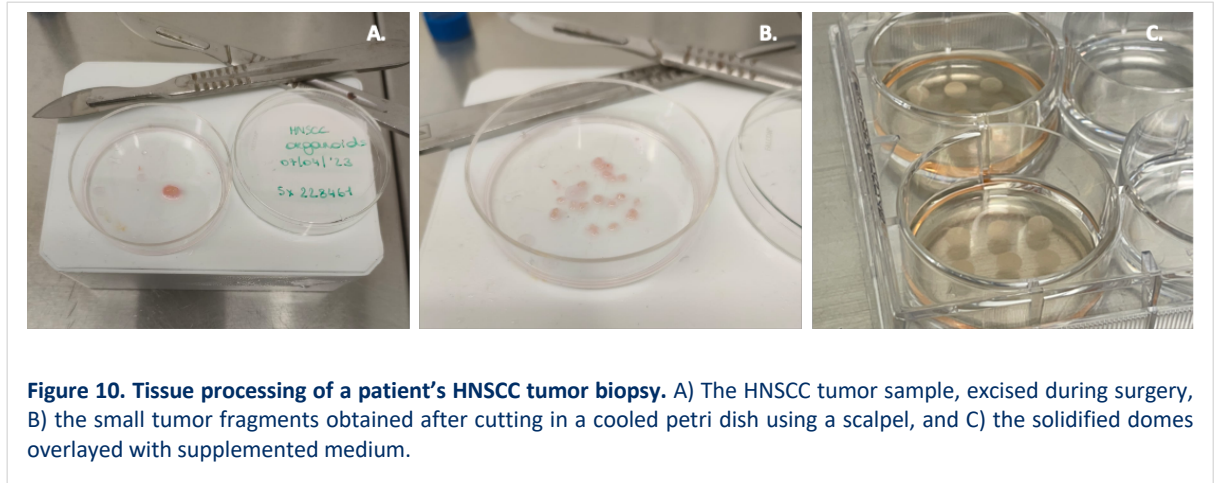
Flow cytometry data was analyzed with the FlowJo™ v10.9 software, and gating strategy was applied to all samples (Figure 9). Briefly, Singlets were retrieved from the Population gating in forward scatter (FSC) and side scatter (SSC) channels; whereafter the viable cell population was selected, and debris was gated out on LIVE/DEAD (Near IR) signal. In this Live Population, cells positive for the violet tracker (violet+, AmCyan) constituted the DC population. DC phagocytosis was captured by the green-positive (green+, FITC) tumor cells within the DC population (double positivity: violet+, green+). Additionally, expression of the activation and maturation markers anti-CD80-PerCPCv5.5, anti-CD83-APC, and anti-CD86-PE-Cv7(Y) were characterized in the violet+ DC population.



7.9 Establishment of Organoid Culture from Fresh Tumor Sample

The patient's HNSCC tumor biopsy, collected during surgery, was stored in full organoid medium supplemented with primocin (Ant-pm-05, InVivoGen) upon processing (max. 1 day, 4°C). For tissue digestion, the sample was placed on a petri dish, refrigerated by a cooling block, and cut in small fragments using a scalpel (Figure 10). The tissue was further digested in 1:1 solution of trypsin (0.25%) and culture medium (max. 60 min, 37°C). The suspension was strained over a 100 µm Easy Strainer Filter (54200, Greiner) to remove undigested fragments, supplemented with Ad-DF⁺⁺⁺ organoid medium (12634, Life Technologies™) (1000 rpm, 5 min, 4°C), and spun down. Red blood cells were subsequently removed with RBC lysis buffer (5 min, RT). After washing in organoid medium, the pellet was resuspended in ice-cold Cultrex growth factor BME Type 2 (3533-010-02, Trevigen). Droplets of 20 µL were plated out on the bottom of a pre-heated 6-well plate, whereafter the plate was inverted to solidify the BME gel in droplet-shaped structures (30 min, 37°C). Finally, the solidified domes were overlaid

with fully supplemented medium containing 12 growth factors (Supplementary Material). To promote organoid formation, 1 $\mu\text{L}/\text{mL}$ of the RHO kinase inhibitor y27632 (10005583, Cayman Chemicals) is added once after each splitting, and incubated.



7.10 Organoid Sub-Culturing and Experimental Preparation

After successful organoid outgrowth, the cultures were split once in 2 weeks, starting minimally 10 days after initial tissue processing. After a thorough washing step with PBS, 1 mL of TrypLE (12604-021, Life Technologies™) was added while disrupting the domes, and incubated (10 min, 37°C). Hereafter, 3 following options arise, depending on the subsequent purpose: (i) **To subculture the organoids into the next passage**, enabling enough space in the domes to maintain their growth, organoids were harvested out of the domes and partially dissociated. Thereby the size of the biggest organoids is reduced. Hereafter, domes were plated out as described above and subsequently incubated until next split. (ii) **For organoid expansion**, tumor incubation was proceeded in the bioreactor CelVivo ClinoStar® (Isogen Lifescience). Therefore, a ClinoReactor® was prepared by hydrating the humidification system (blue water beads in the outer circle of the bioreactor), and coating of the inner reaction chamber with bovine serum albumin (BSA) to avoid tissue adhesion. Hereafter, a suspension of partially dissociated organoids was injected in the reactor, topped with fully supplemented organoid medium until a total volume of 10 mL, and incubated in the ClinoStar® (Figure 11A). (iii) **When organoids are split for experimental preparation**, they must be fully dissociated to single cell level in order to perform a cell count. Domes were thereupon plated out in 150,000 cells/dome to ensure uniform growth and organoid size, and incubated (4 days, 37°C). If a successful growth was accomplished, 4-days old organoids were used for experimental purposes (Figure 11B).

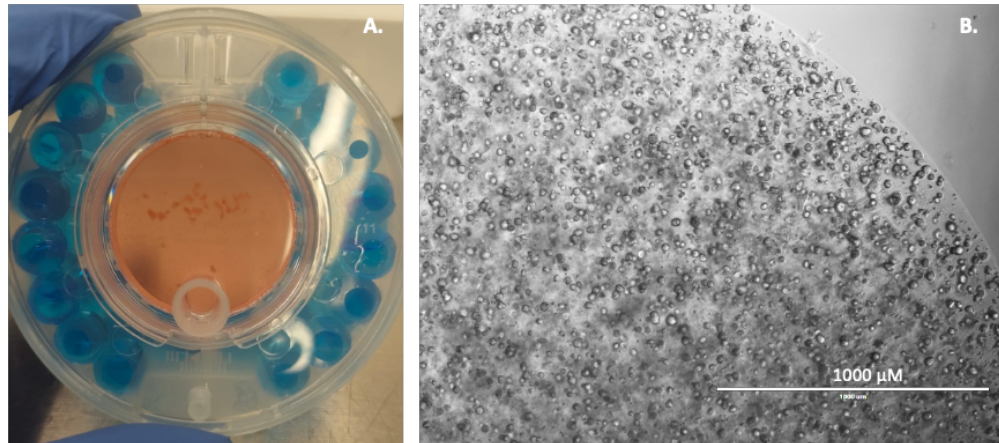


Figure 11. Organoid expansion and experimental plating out. A) The injected organoid sample in the ClinoReactor®, surrounded by water-filled beads for hydration, for optimal organoid expansion, B) 4-day old organoids at 150,000 cells/dome for experimental purposes.

7.11 Harvesting and Experimental Handling of Organoids

For experimental read-outs, organoids were plated out in in-house prepared, pre-coated 96-well plates. A cooled, flat-bottomed 96-well plate was covered with 30 μL /well Cultrex, centrifuged (1500 rpm, 5 min, 4°C), and subsequently incubated (30 min, 37°C) for gel solidification. Meanwhile, 4-days old organoid domes were carefully washed with PBS and gently disrupted with cold organoid harvesting solution (shaking on ice, 15 min), dissolving Cultrex domes while preventing organoid dissociation. The organoids were collected in a 0.1% BSA/PBS pre-coated 15 mL tube and spun down (1000 rpm, 5 min, 4°C); whereafter the pellet was dissolved in 1000 μL full medium.

Organoid count was retrieved from the Spark® Cyto: 45 μL PBS was pipetted into a flat-bottomed 384-well counting plate (3764, Corning®) to which 5 μL organoid suspension was added. Measurement was conducted in triplicate to determine the mean organoid count ($[\text{mean } 3 \text{ wells}] * 200 = \# \text{organoids/mL}$). Seeding the organoids, a density of 1,500 organoids/well in 100 μL was recommended. Organoid suspension was added to the previously coated, solidified plate and gently spun down (1000 rpm, 2 min). Overnight incubation was performed to enable organoid attachment to the coating layer.

Organoids were treated as described above with a 7-point titration of CIS and/or different NTP features. Live-cell imaging was performed in the Spark® Cyto by continuous scanning every 4h for 3 days to measure tumor kinetics. In addition, organoid cell death was examined using IncuCyte® Cytotox Green Reagent (4633, Essen BioScience).

7.12 Statistical Analysis

Membrane marker experiments were repeated thrice, with 5 spheroids per repeat, for all cell lines (n=10-15). Analysis of secreted factors was performed 3 times per timepoint. Supernatant of spheroids within the same condition was pooled together and measured in duplo for ATP and in triplo for HMGB1 (n = 3 per timepoint). DC co-culture experiments were minimally performed 4 times with 4 independent donors (n = 4-5). Relative expression was determined for the surface-presented DAMPs, while released factors and phagocytosis were represented in fold changes. For the flow cytometric analysis of DC maturation and activation markers, the difference in mean fluorescence intensity (ΔMFI) between treated samples and the untreated control sample was calculated ($\Delta\text{MFI} = \text{MFI}_{\text{treated}} - \text{MFI}_{\text{untreated}}$). Statistical analysis was conducted in JMP® Pro 16.0.0 Statistical Software using linear mixed models with a Tukey's post-hoc test to correct for multiple comparisons. Data in the figures were presented as mean \pm standard error mean (SEM). Significance was accepted when $p \leq 0.05$. No statistical analysis was conducted on preliminary organoid data. Graphical representations were created in GraphPad Prism9.

8 Results

8.1 Surface-Presented DAMPs Increased After NTP-CIS Combination Therapy

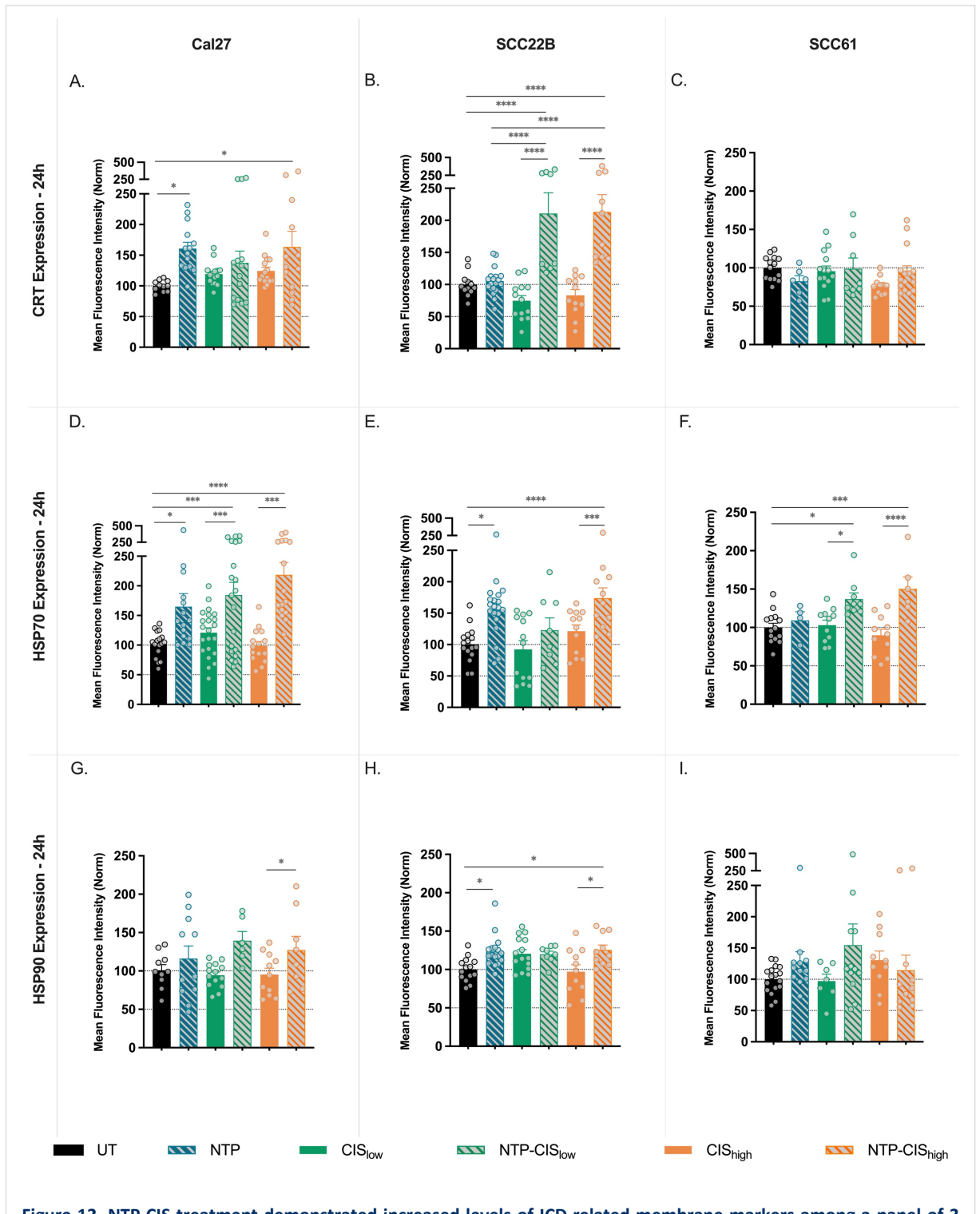
To investigate whether the combined application of NTP and CIS was able to increase immunogenic marker expression on the cell-surface of cancer cells, 3 membrane-associated ICD markers were assessed 24h after therapy application. Spheroids of 3 different HNSCC cell lines (Cal27, SCC22B, and SCC61) were treated with NTP and CIS, both as a monotherapy, and as a combination; whereafter CRT, HSP70, and HSP90 levels were evaluated with immunofluorescence imaging. Mean fluorescence intensities, normalized to UT controls, were assessed after image analysis.

For the SCC22B cell line, no significant effects on CRT were observed after NTP or CIS_{low/high} monotherapy. However, CRT levels increased by 2- and 3-fold when CIS chemotherapies were combined with NTP (210.6 ± 32.3 and 213.2 ± 26.9 , low and high dose, respectively), compared to the UT condition ($p < 0.0001$) and both CIS_{low} (74.62 ± 8.2 ; $p < 0.0001$) and CIS_{high} (83.3 ± 8.9 ; $p < 0.0001$) monotherapy controls (Figure 12B). CRT expression in the Cal27 cell line significantly increased compared to UT after NTP (160.9 ± 10.3 ; $p=0.0437$) and after combined application with CIS_{high} (163.6 ± 25.4 ; $p = 0.0473$) (Figure 12A). Although significant changes were not measured in Cal27 or SCC61 CRT expression after NTP-CIS combination therapy, relative to NTP or their CIS monotherapies, a trend in increased CRT levels was reported (Figure 12A, C).

NTP exerted a promoting effect on HSP70 expression among all cell lines (Figure 12D-F). For Cal27, HSP70 was significantly upregulated for all treated conditions with NTP (alone or in combination), compared to UT. Moreover, both combination strategies (NTP-CIS_{low/high}) showed significantly higher levels of HSP70 compared to their CIS monotherapy (121.0 ± 8.4 ; $p = 0.0008$ and 98.9 ± 7.4 ; $p = 0.0007$, low and high CIS, respectively) (Figure 12D). Similar results were measured for HSP70 expression in the SCC22B and SCC61 cell lines (Figure 12E-F).

More moderate treatment effects were measured for HSP90 expression, where only the SCC22B cell line demonstrated significant increase in HSP90 expression following NTP monotherapy (123.5 ± 5.0 ; $p = 0.0226$) (Figure 12H). Moreover, NTP-CIS_{high} combination treatment demonstrated an increase in HSP90 expression for both Cal27 (127.3 ± 17.8) and SCC22B (125.5 ± 6.6), compared to their corresponding CIS_{high} monotherapy (95.4 ± 8.2 ; $p = 0.0457$ and 97.3 ± 9.0 ; $p = 0.045$, respectively) (Figure 12G, H).

In summary, our data revealed a clear effect of NTP application on surface-presented DAMP expression in different HNSCC cell lines, which is indicative of increased immunogenicity. Moreover, it is apparent that the addition of NTP to several CIS regimens in a combinatorial setting can further elevate membrane-associated DAMP signaling, thereby suggesting the promotion of ICD induction. In the next experiments, we aimed to further explore the immunogenic capacity of the combination strategies by evaluating the cell-secreted and released DAMPs.



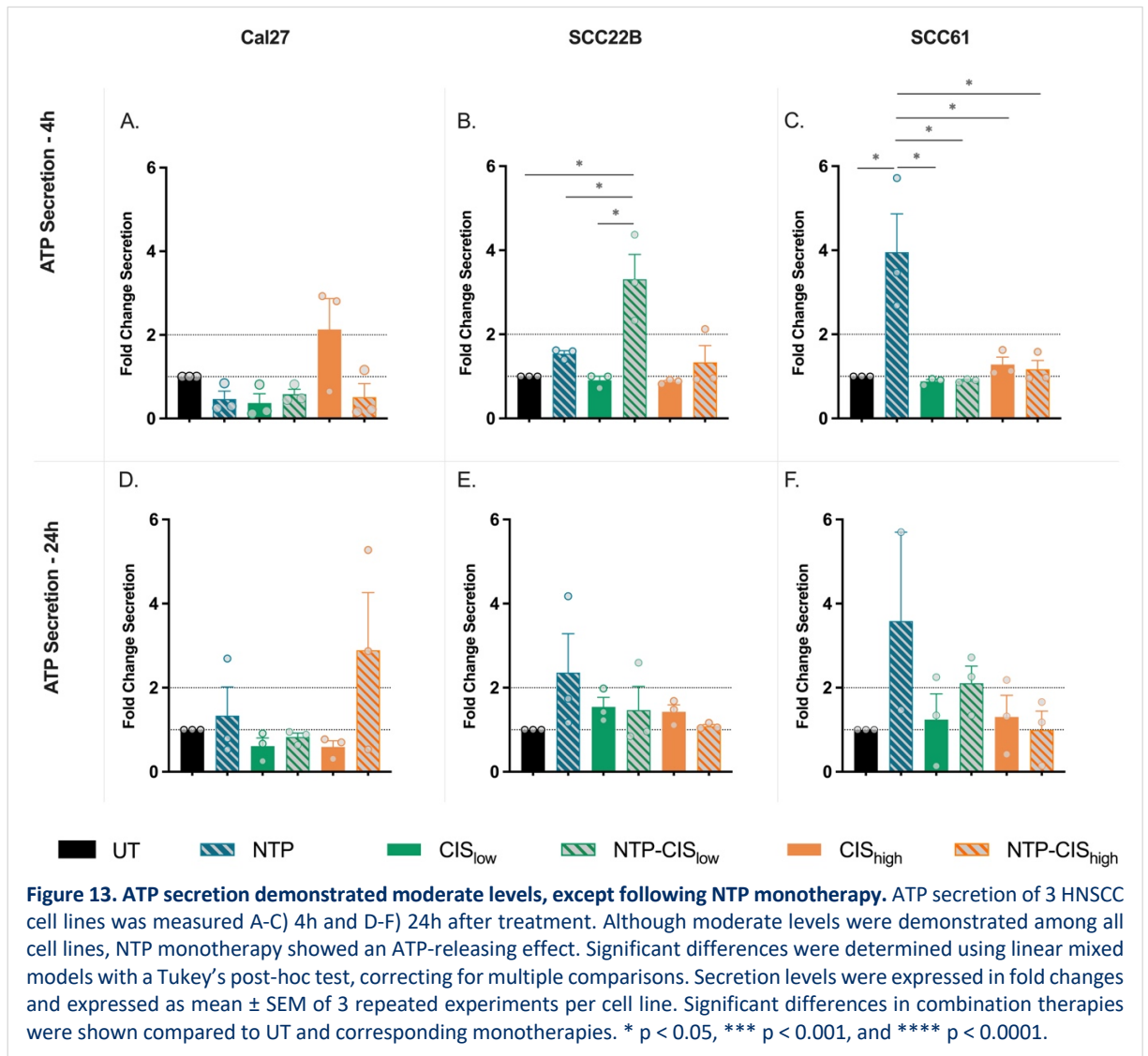
8.2 ATP Secretion Increased After NTP Monotherapy

In addition to membrane-related markers, we evaluated whether CIS chemotherapy in combination with NTP could amplify the secretion or release of immunogenic markers. In that regard, HNSCC spheroids of Cal27, SCC22B, and SCC61 were treated with NTP and/or CIS chemotherapy and their liberated ATP and HMGB1 levels were subsequently evaluated in the supernatant. The levels of these molecules in the supernatant were expressed in fold changes, relative to the UT condition.

The release of ATP in the extracellular space is known to occur rather early after ICD induction^[78]. Therefore, we assessed the spheroid-secreted ATP for 3 HNSCC cell lines at 4h and 24h after treatment, using a bioluminescent assay. Neither of the CIS treatment concentrations increased ATP secretion at the observed timepoints (Figure 13), while NTP alone was only effective for the SCC61 cell line at 4h post treatment. In this case, NTP monotherapy significantly increased ATP secretion (4.0 ± 0.9) compared to the UT condition ($p = 0.0018$) and both the CIS_{low} (0.9 ± 0.0 ; $p = 0.0013$) and CIS_{high} monotherapies (1.3 ± 0.2 ; $p = 0.0038$) (Figure 13C).

For the SCC22B cell line, a strong elevation was reported for the NTP-CIS_{low} treatment (3.3 ± 0.6) compared to the UT condition ($p = 0.0039$) at 4h post treatment. Furthermore, this combination strategy elicited a 2-fold increase in ATP compared to NTP monotherapy (1.5 ± 0.1 ; $p = 0.0228$), and even a 3.5-fold increase compared to CIS_{low} monotherapy (0.9 ± 0.1 ; $p = 0.0029$) (Figure 13B). These effects were diminished at 24h post treatment, wherein only NTP monotherapy showed an increasing trend, relative to UT (2.4 ± 0.9 ; $p = 0.3696$) (Figure 13E).

Overall, NTP triggered variable ATP release in all cell lines at 4h (Figure 13A-C), but any effect returned to baseline at 24h (Figure 13D-F). Thus, ATP secretion in response to NTP appeared to be early and cell line specific. To further explore the DAMPs present in the supernatant following therapeutic ICD induction, we hereafter observed the effects of the NTP-CIS combination therapy on the release of nucleus-resident HMGB1.

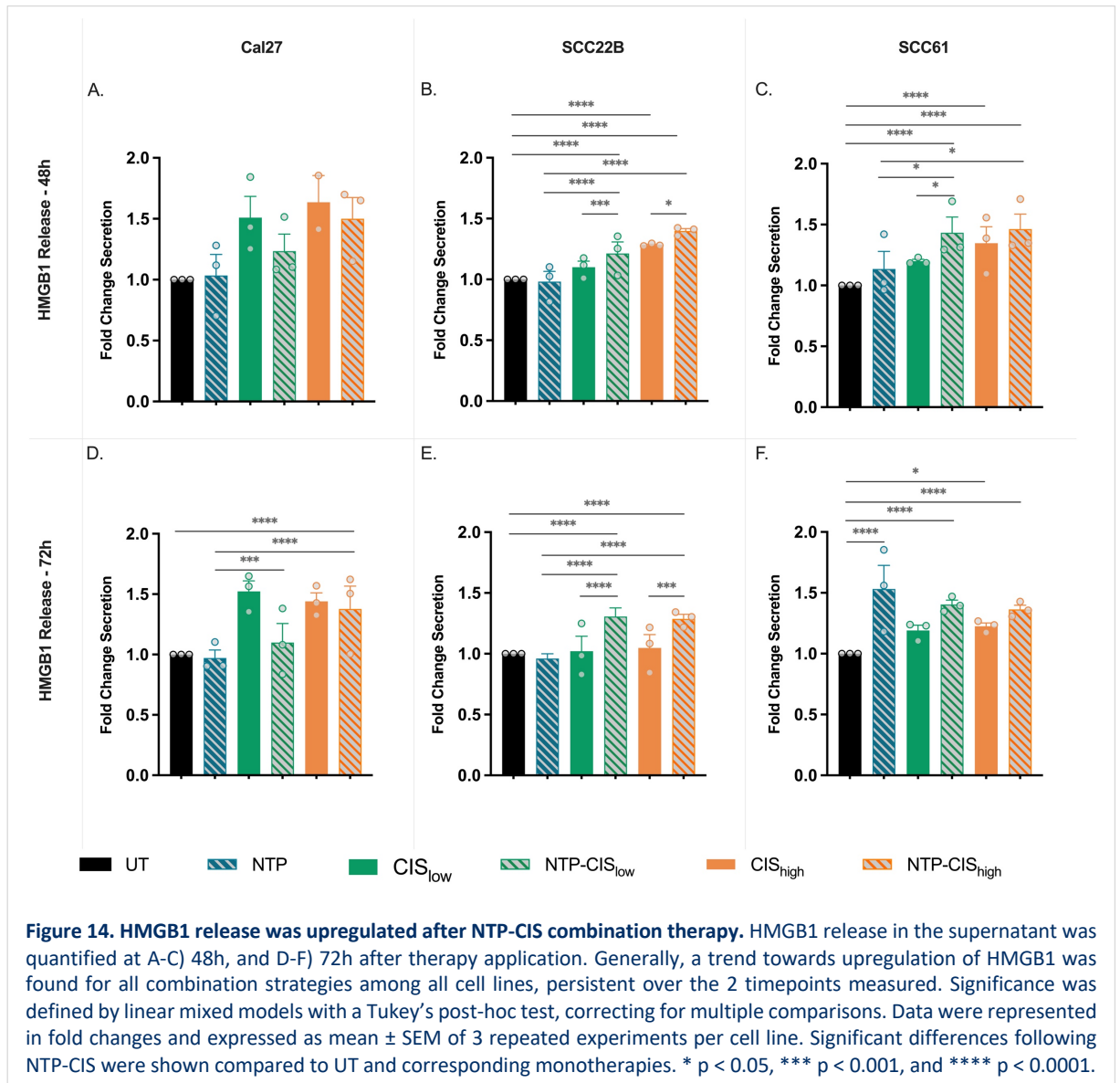


8.3 HMGB1 Release Increased Following Combined NTP-CIS Therapy

As a late-stage marker of ICD induction^[78], HMGB1 secretion was assessed in all 3 HNSCC cell lines at 48h and 72h after treatment (Figure 14). NTP monotherapy exerted a positive influence on HMGB1 release in SCC61 cells, 72h after treatment (1.5 ± 0.2 ; $p < 0.0001$) (Figure 14F), whereas HMGB1 release from other cell lines remained moderate, when compared to that of the UT (Figure 14A-E). For both the SCC22B and SCC61 cell line, NTP combined with CIS_{low} (1.2 ± 0.2 and 1.4 ± 0.1 , SCC22B and SCC61, respectively) or CIS_{high} (1.4 ± 0.0 and 1.5 ± 0.1) resulted 48h after treatment in significantly higher levels of HMGB1 in the supernatant compared to UT ($p < 0.0001$). In addition, HMGB1 levels showed a significant increase in the NTP-CIS_{low/high} combinations compared to corresponding CIS and NTP monotherapies, 2 days post treatment (Figure 14B, C). These significant effects were maintained up to 72h in the SCC22B cell line, for both the low (1.3 ± 0.1 vs 1.0 ± 0.1 ; NTP-CIS_{low} vs CIS_{low}; $p < 0.0001$) and high (1.3 ± 0.0 vs 1.0 ± 0.1 ; NTP-CIS_{high} vs CIS_{high}; $p = 0.0006$) combinatorial regimens (Figure 14E), while an increasing trend was still reported for SCC61 cells (Figure 14F).

HMGB1 levels in Cal27 remained rather moderate 48h after treatment (Figure 14A), with after 72h an upregulation of liberated HMGB1 in the 2 NTP-CIS combinations compared to NTP monotherapy (Figure 14D). Overall, our data demonstrated a persistent profile of HMGB1 release, retained up to 72h after treatment for

different HNSCC cell lines. Interestingly, combined NTP-CIS application boosted the release of HMGB1 compared to the monotherapies, highlighting the potential to evoke another hallmark of ICD induction. Taken together, there is mounting evidence that NTP in combination with CIS at low and high concentrations could enhance DAMPs emission (surface-bound and released), which could improve subsequent anti-tumor immunity. Therefore, in the following experiments, we aimed to investigate immunological functionality of the emitted DAMPs following combination treatment, by conducting co-culture experiments with immune cells.



8.4 NTP-CIS Combination Therapy Improved DC Phagocytosis and Expression of Activation and Maturation Markers

A critical step in the initiation of an effective anti-tumoral response is the engagement of the selective engulfment and processing of tumor cells by APCs (e.g., DCs)^[53]. In that regard, the 3 HNSCC spheroids were pre-treated as before and co-cultured with iDCs, derived from healthy donors' blood, to examine their phagocytotic capacity and state of maturation. The detailed gating strategy is provided above (Figure 9).

The PKH67+ spheroids were incubated with DCs for 48h and were imaged with the Spark® Cyto in brightfield (Figure 15A-D) and green fluorescence (Figure 15E-H) channels. By merging the channels, treatment-related effects on DC phagocytosis could be visualized by the overlap of green-fluorescent tumor cells in the DCs (Figure 15I-P). Comparing the areas of interest (zoomed-in), co-cultures of UT or CIS_{high} treated spheroids showed limited green tumor cell – DC overlap, indicating minimal phagocytosis (Figure 15M, N). Interestingly, NTP monotherapy demonstrated more of these overlapping events, while the highest amount was visualized following the NTP-CIS_{high} combination (indicated by arrows) (Figure 15O, P). These pictures visually substantiate the enhanced DC uptake of tumor cells after NTP-including treatment applications.

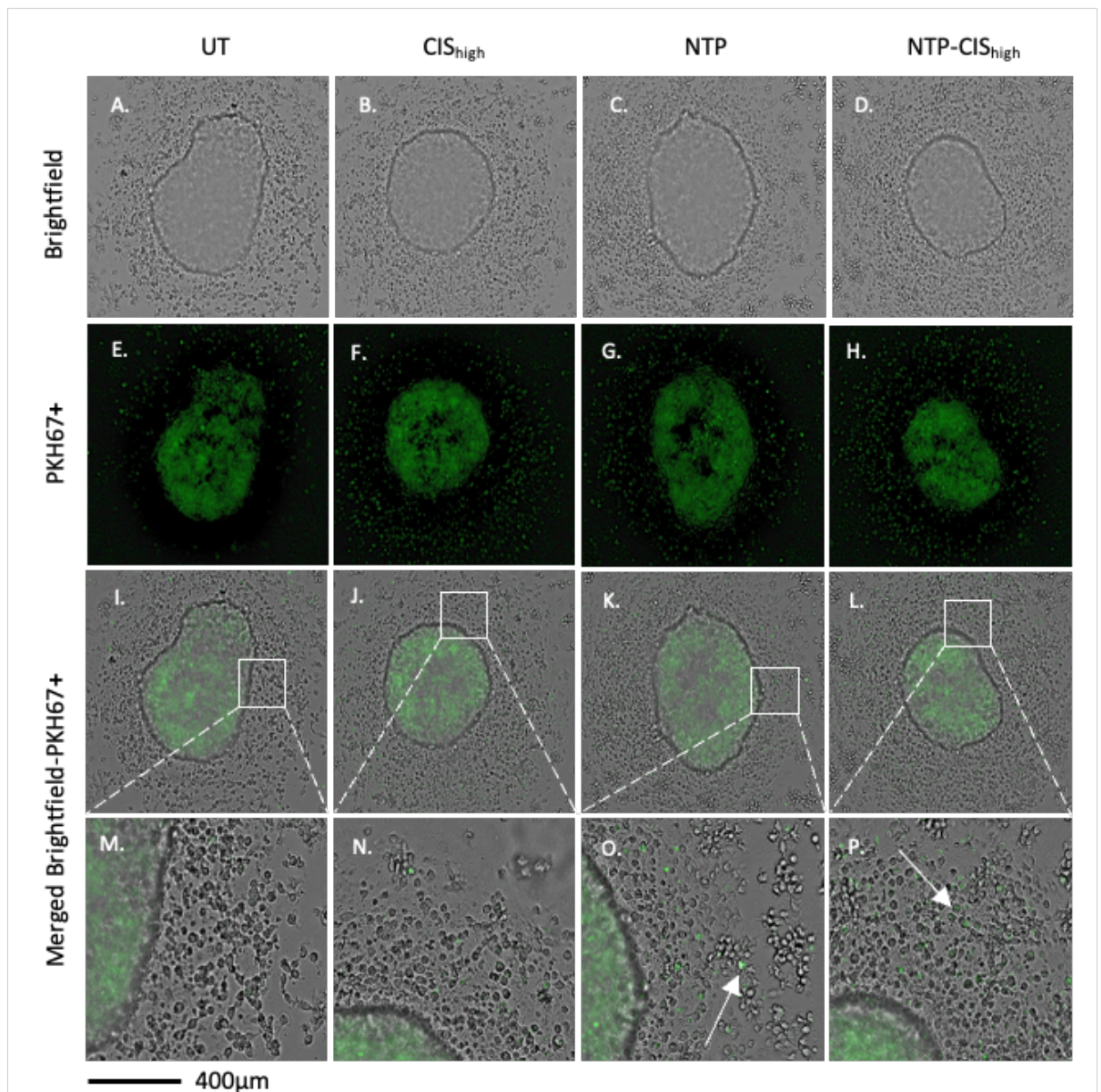


Figure 15. Phagocytotic capacity of tumor cells visually increased after NTP-CIS_{high} treatment during DC co-culture. PKH67+ HNSCC spheroids were incubated for 48h with healthy donor-derived DCs. Hereafter, images were taken on the Spark® Cyto of spheroids, challenged with different treatment regimens (UT, CIS_{high}, NTP, and NTP-CIS_{high}). A-D) Brightfield, E-H) PKH67+, I-L) merged brightfield-PKH67+, and M-P) zoomed, merged brightfield-PKH67+. The squares indicated the zoomed-in area, while the arrows showed a phagocytosed tumor cell.

To further investigate the DCs' functionality, we aimed to quantify the phagocytotic potential by capturing the engulfment of PKH67+ tumor cells by VioletTracker+ DCs during flow cytometry analysis (double positivity: violet+, green+). Fold changes of DC phagocytosis were calculated to the UT condition.

Both CIS_{high} and NTP were able to enhance the levels of tumor cell uptake as monotherapy in all 3 HNSCC cell lines (Figure 16A-C), with phagocytosis increasing with approximately a 1,5-fold for NTP and 2-fold for CIS_{high}, relative to the UT condition. Interestingly, once NTP and CIS were applied in combination, engulfment peaked after NTP-CIS_{high} administration, demonstrated by a 2- to 3-fold upregulation compared the UT level (2.4 ± 0.2 ; $p < 0.0001$ for Cal27, 2.1 ± 0.4 ; $p = 0.0086$ for SCC22B, and 2.7 ± 0.6 ; $p = 0.0017$ for SCC61). Additionally, a comparable trend was seen when NTP was combined with lower concentrations of the chemotherapeutic. Thus, in general, an increasing trend of phagocytosis was seen among all 3 HNSCC cell lines following combined application of NTP and CIS_{low/high}.

Besides their role in phagocytosis and thereupon antigen presentation, mDCs play an important role in forwarding danger-associated information to the adaptive immunity (e.g., T cells) via the presence of co-stimulatory signals on the cell-surface, which subsequently enhances the specific anti-tumoral response^[55]. Hence, the expression pattern of several phenotypic DC markers will alter during the activation and maturation process. In the regard of better understanding the effects of the novel NTP-CIS combination strategy on DC functionality, we assessed the expression levels of the co-stimulatory markers (i.e., CD80, CD83, and CD86) in 3 different HNSCC spheroids upon co-culture. Expression levels were described as Δ MFI, with MFI_{untreated} subtracted from MFI_{treated}.

Although significant differences were not observed in maturation marker expression, an increasing trend after NTP-including treatments was visualized (Figure 16D-L). NTP monotherapy tended to elevate CD80 expression in Cal27 and SCC22B cells, while an increase in marker expression was seen when NTP was added to both low and high CIS regimens, in all cell lines (e.g., 206.5 ± 102.8 vs 495.5 ± 220.1 for Cal27, CIS_{high} vs NTP-CIS_{high}, respectively) (Figure 16D-F). Although no treatment-related effects on CD83 were reported in the SCC61, expression of this marker was stimulated in all NTP-including treatments for the other 2 cell lines (Figure 16 G-I). Illustrative, CD83 levels in the Cal27 cell line were multiplied with 5.6- and 3-fold after both NTP-CIS_{low} and NTP-CIS_{high} combinations, respectively (3651.0 ± 1741.0 and 2721.5 ± 1074.0), in comparison to their CIS monotherapy counterpart (652.5 ± 1298.0 for CIS_{low} and 882.8 ± 1019.0 for CIS_{high}) (Figure 16G). Similar results were observed regarding SCC22B (Figure 16H). Moreover, NTP as monotherapy seemed to have a positive effect on the expression of the CD86 maturation marker on DCs for 2 out of the 3 tested cell lines (Figure 16J, K), which was further highlighted when NTP was added to both the low and high chemotherapeutic regimes.

Taken together, the increased levels of phagocytosis after NTP-CIS combination strategy are demonstrative for enhanced tumor cell recognition and engulfment. In addition, our data suggested that NTP exerted a promoting effect on the activation and maturation process of DCs.

These findings are important steps in supporting our rationale and underline the potential of NTP-CIS combination therapy to stimulate multiple aspect of the cancer-immunity cycle; this to eventually engage the adaptive immunity and provoke lasting anti-tumoral effects.

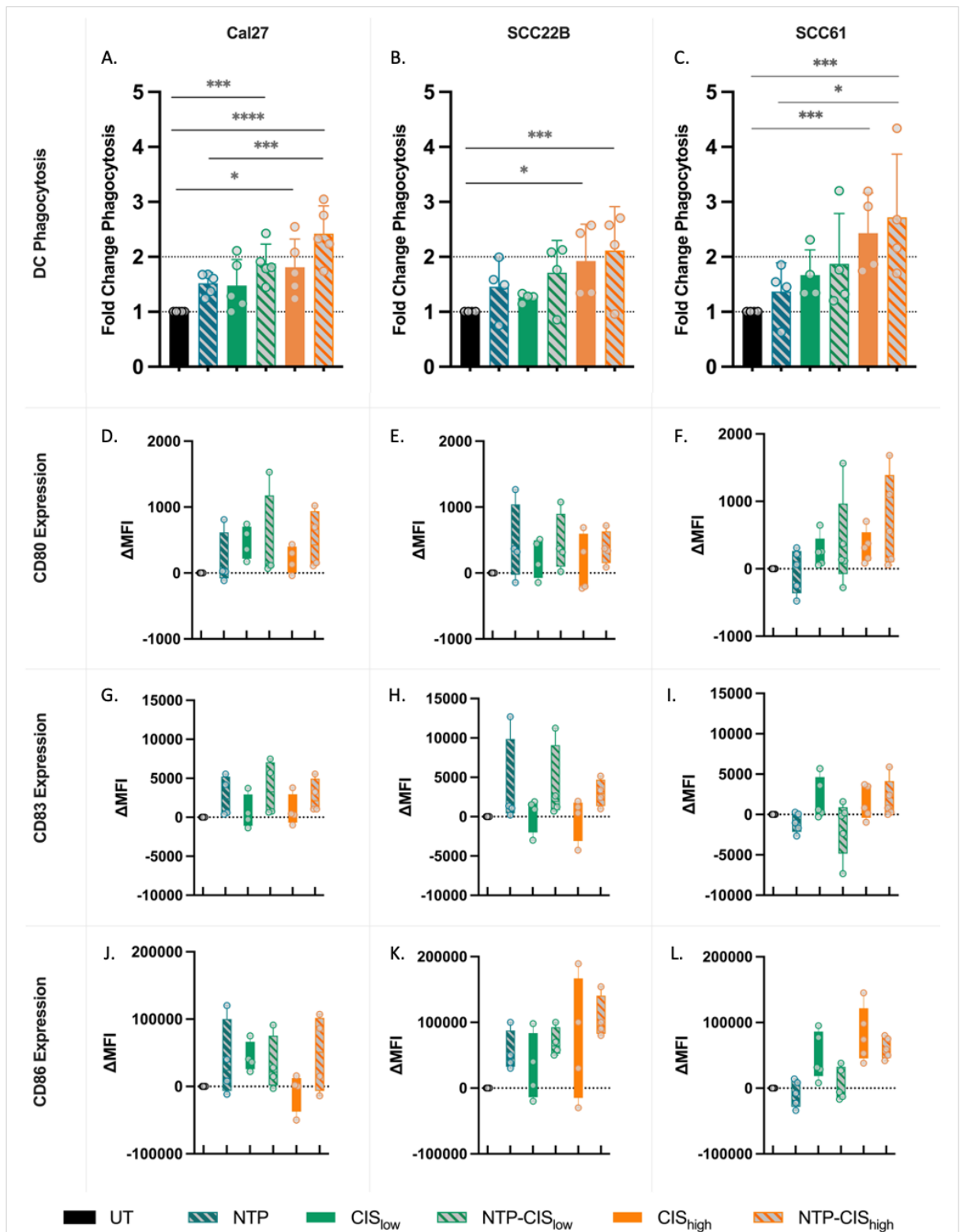


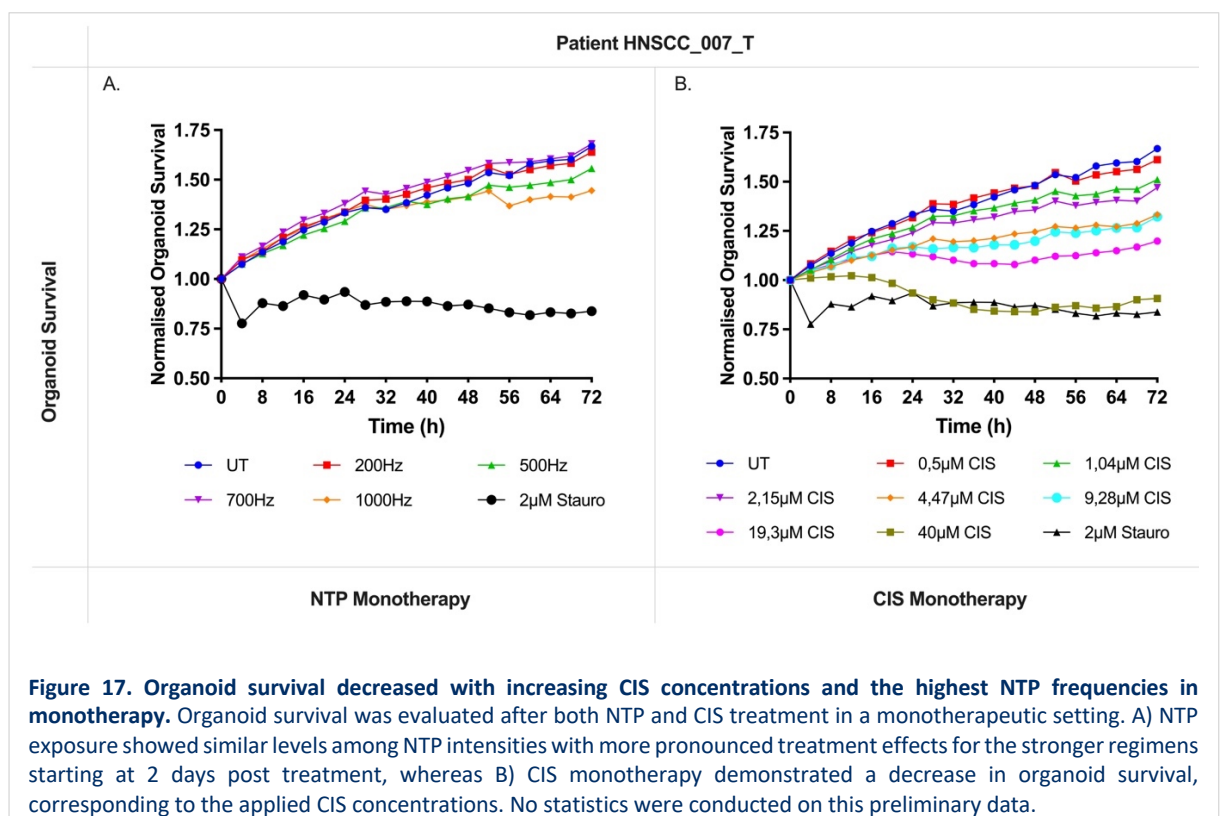
Figure 16. More effective DC phagocytosis and expression of activation and maturation markers after NTP-CIS combined application. Pre-treated spheroids of 3 different HNSCC cell lines were co-cultured with DCs. A-C) Fold changes of phagocytosis, relative to UT, were obtained after flowcytometric analysis, measuring the double positives (green+, purple+). Among the 3 cell lines, a trend toward significance for the combination therapies was distinguished. D-L) Although no significant differences were seen in the expression patterns of CD80, CD83, and CD86, NTP exerted generally stimulating effects. Significance was defined by linear mixed models with a Tukey's post-hoc test, correcting for multiple comparisons. Data were represented in fold changes and expressed as mean \pm SEM of 4-5 repeated experiments per cell line. Significant differences in the combinatorial setting were, shown compared to UT and corresponding monotherapies. * $p < 0.05$, *** $p < 0.001$, and **** $p < 0.0001$.

8.5 Patient-Specific Therapy Response Validated in HNSCC Organoids

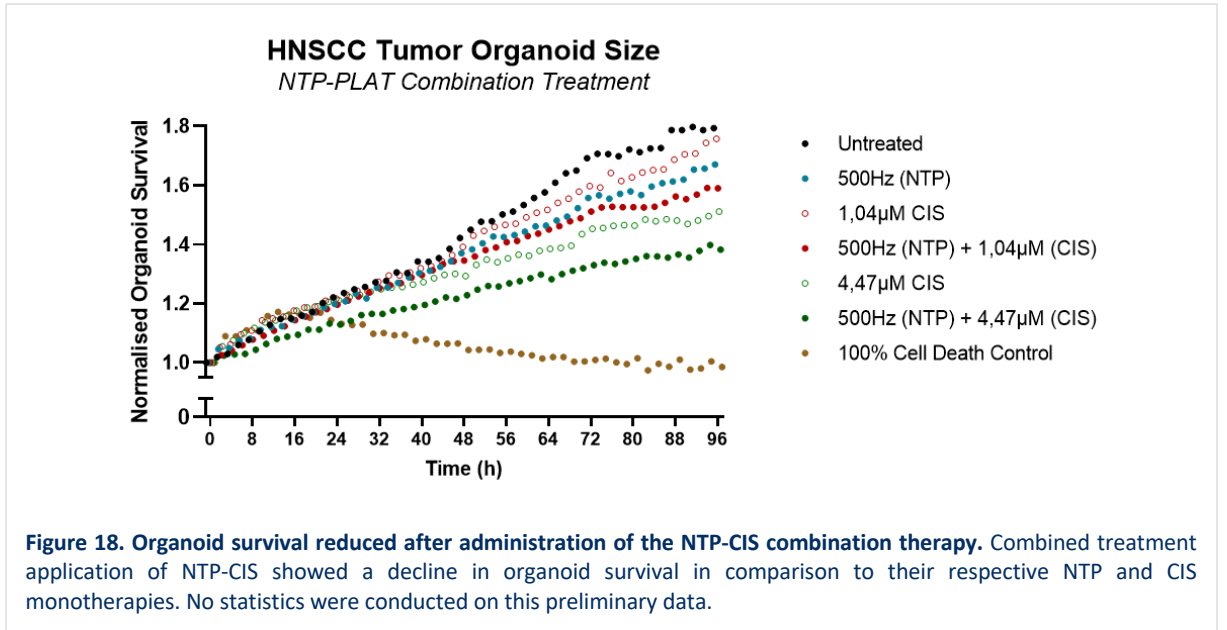
Previous results discussed the effects of the NTP-CIS combination strategy on ICD induction via DAMP release and DC immune activation, evaluated in HNSCC 3D spheroids. To bridge the gap between *in vitro* experiments and application in an *in vivo* or clinical setting, we initiated the validation of our treatment effects in HNSCC PDOs. This ‘patient-in-the-lab’ model enables treatment evaluation in a tumoral environment uniquely resembling the phenotypic and genotypic characteristics of the original tumor^[136]. Our lab has extensive experience in PDO research and was able to establish an organoid biobank of 7 HNSCC patients, which holds great promise to screen and optimize NTP and CIS application against a variety of HNSCC-specific tumoral signatures, with the ultimate goal of introducing patient-matched therapies and treatment recommendations in the clinic.

As pilot outline for further combinatorial research, we aimed to screen various NTP frequencies and CIS concentrations as monotherapy, in here specifically for the HPV-negative patient HNSCC_007_T (Figure 17). After treatment application, the organoids on the coated 96-well plate were imaged with the Spark® Cyto, taking consecutive scans every 4h, up to 72h post treatment. Organoid survival was determined by subtracting the Incucyte® Cytotox green ‘cell death’ organoid area from the brightfield ‘live’ organoid area, for each timepoint respectively. Intra-well normalization was performed for all signals to account for organoid abundance and size at the treatment starting point. Staurosporin was used as positive control for cell death (100%).

Evaluating the preliminary results on organoid survival following NTP monotherapy exposure, no major therapeutic impact was observed among the different NTP frequencies tested (Figure 17A). However, at later timepoints (48h post treatment), organoid growth seemed to be stalled when higher intensities were applied (500 Hz and 1000 Hz). In parallel, the initial findings from the CIS monotherapy titration demonstrated a dose-dependent decline in organoid survival, which was maintained over the 72h of treatment evaluation (Figure 17B).



When the patient-specific response to the monotherapeutic regimes is determined, several NTP-CIS options will be considered to explore the combinatorial potential of the 2 agents. Demonstrative for this, the HPV-positive patient HNSCC_001_T was previously screened in our lab for selected NTP-CIS combinations after analyzing monotherapeutic responses (Figure 18). These results showed a greater decline in organoid survival after both combination therapies, related to their monotherapeutic counterparts.



9 Discussion

Despite considerable progress in therapeutic approaches, HNSCC remains a hard-to-treat cancer type. Many patients relapse or develop distant metastasis (R/M HNSCC), facing a devastating prognosis. Additionally, current treatment methods present low response rates and are inseparable from severe side effects. Hence, there is still an unmet need to find new treatment modalities to help patients diagnosed with (R/M) HNSCC.

Recently, a lot of research goes to anti-cancer strategies with immune-stimulating properties and the ability to provoke a durable anti-cancer response, including ICD-inducing agents (e.g., chemotherapy and radiotherapy). This therapeutic approach intervenes at the front-end part of the cancer-immunity cycle, boosting the initial immunological steps via DAMP and tumor Ag release, to initiate the amplification of a specific anti-cancer response.

The past decade, NTP emerged as an attractive new modality for cancer therapy, with special interest in its immunogenic capacities. Our lab has built-up a broad expertise in NTP application for cancer therapy, and we recently reported that ICD induction by NTP is mainly elicited by the generated short-lived reactive species^[87]. In parallel, the immunogenic capacities of currently-established therapies are reconsidered. In that light, the general consensus that chemotherapeutic agents are non-immunogenic is revised: conflicting data have been reported regarding the ability of CIS to induce ICD by ER stressing^[84, 141], which was expected to prohibit CRT translocation to the cell membrane. However, ICD induction by chemotherapy seems to be dose-dependent, since CIS has been reported to exert more immunogenic properties when administered in lower, sublethal concentrations, by stimulating more ER stress, than the classical high doses^[142].

As both HNSCC standard of care chemotherapy (CIS) and NTP demonstrated ICD induction via ER stress in monotherapy, the combination of CIS and NTP may overload the cellular stress mechanisms, resulting in a higher DAMP release and immunogenicity. To explore this, our study aimed to unravel the immunogenicity of the novel NTP-CIS combination treatment strategy by evaluation of DAMP release and functional DC immunity in advanced 3D tumor models for HNSCC, in the interest of an improved clinical strategy to increase therapy efficacy of current HNSCC standard of care treatments.

Thorough research has identified various ICD markers that can be induced by therapeutic intervention^[78]. Interestingly, it is reported that the nature of the ICD inducer is decisive for which DAMPS will be released: both chemotherapeutic and physical intervention have been previously reported to induce overlapping ICD hallmarks, including ATP, CRT and HMGB1; while other DAMPs (e.g., HSPs) and inflammatory cytokines (e.g., type I interferon (IFN)) are also frequently present in the process of dying tumor cells^[78]. In that regard, we selected a panel of 5 key ICD markers to be evaluated: membrane-associated CRT, HSP70, and HSP90; and supernatant-released ATP and HMGB1. Given that the ICD-triggered presence of these hallmarks has been earlier reported in CIS as well as in NTP monotherapy, it seemed intriguing to investigate if the 2 modalities together were able to provide an amplified ICD profile.

To enable a rationally-designed combination, both NTP intensities and CIS concentrations were previously screened in monotherapy, at our lab. NTP characteristics were assessed testing different frequencies (Hz) for variable durations in time (sec). It was found that treatment properties of 1000 Hz for 10 sec (10,000 cycles) were able to kill 25% of exposed tumor cells up to 48h after treatment. Besides this, optimal CIS chemotherapy concentrations were selected through a 7-point titration, ranging from untreated controls until 80 μ M (0-100% killing capacity). Hereafter, 2 working concentrations were chosen, specific for each cell line: (i) a low concentration (CIS_{low}) that resulted in minimal cell death after 24h and increased to 25% of cell death 48h post treatment; and (ii) a high concentration (CIS_{high}) that induced cell death percentages of 25% and 50%, at 24h and 48h, respectively; while taking into account the CIS serum levels present in the patient, in the context of clinical relevance^[141]. From this, 2 NTP-CIS combinations per cell line (NTP-CIS_{low} and NTP-CIS_{high}) were used throughout the entire course of this thesis. Of note, it is essential to encounter the right timepoints for analytic measurements: NTP application is known to affect cancer cells shortly after exposure, whereas CIS effects peak more slowly (2 days post treatment *in vitro*); to capture combined treatment effects, an adequate read-out window between 4h up to 72h was defined.

To profoundly investigate the immunogenic landscape in HNSCC after combined application of NTP and CIS, we first assessed treatment-related effects on the 5 included ICD markers. Our results demonstrated higher CRT

expression among all HNSCC cell lines after combined NTP-CIS treatment strategy (Figure 12A-C), although differences appeared to be cell line specific. Remarkably, a 3-fold increase was reported compared to CIS monotherapy, suggesting NTP's promoting capacity as a mean to overload cancer cells with ER stress and multiply DAMP release. The chaperone proteins HSP70 and HSP90 are also closely linked to ER stress, upregulated to assist in the removal of misfolded proteins^[76]. Recently, Tsutsumi et al. reported increased levels of HSP90 upon CIS monotherapy in an *in vitro* model of OPSCC^[143]. Our results confirmed the same HSP90 presence, with a moderate increase after combination with NTP (12G-H). The same research group described that HSP70 expression was not altered in the same CIS monotherapeutic setting. Interestingly, our strategically-designed combination revealed a 2-fold increase in HSP70 levels, compared to CIS alone (Figure 12D-F), which confirms the ability of NTP to boost to ICD induction of CIS chemotherapy.

Overall, our results on membrane-associated ICD markers showed an increased DAMP expression upon combinatorial treatment of NTP and CIS. These findings suggest that boosting ER stress with additional NTP application can consecutively lead to more danger signals that enable better recognition of malignant cells by the immune system.

Hereinafter, we aimed to assess the ICD-associated release of DAMPs in the supernatant, one such is ATP secretion. The increased extracellular amount of ATP upon ICD induction is known to act as a key initiator of a profound immunogenic responses^[78]. Since killed cancer cells will burst by therapeutic intervention, intracellular non-immunogenic ATP will be released in the process. Emphasizing timely measurement prior to cell rupture, we set 2 early detection timepoints (4h and 24h post treatment). Previously conducted cell viability assays confirmed our chosen timepoints with minimal decreases in intracellular ATP at 24h post treatment. Our results suggested particularly NTP sensitization in 2 out of 3 cell lines, SCC22B and SCC61, but increasing amounts after combination therapy were not observed (Figure 13). The peak in extracellular ATP secretion, especially observed post NTP exposure, can be devoted to differences in the required time for treatment modalities to perform effects; the early ICD-inducing impact of NTP is thus demonstrated, whereas it takes longer for CIS to halt cellular processes and create DAMP release. Confirming this, Golden et al. did show *in vitro* an amplified increase to monotherapy in ATP secretion 24h after a combination of platinum-based chemotherapy and radiotherapy^[82].

Next, we evaluated the translocation of nucleus-resident HMGB1 to the supernatants upon NTP-CIS treatment. Chavez-Dominguez et al. demonstrated that CIS monotherapy was able to induce release of HMGB1, in *in vitro* lung adenocarcinoma cell lines^[144]. In response, our findings revealed a consistent upward trend in release of HMGB1 levels into the cytoplasm after CIS concentrations, especially when combined with NTP, underlining the role of RONS as a key player in boosting HMGB1 levels^[145]. This increased liberation of "find-me" signals may suggest an acceleration in the engagement of immune cells, e.g., DCs, promoting tumor cell clearance.

Taken together, NTP exposure in monotherapy affected ATP secretion profoundly, demonstrative for its early cellular impact. Besides this, HMGB1 was especially released after combined application of NTP-CIS. Boosting the induction of both surface-exposed and released DAMPs may facilitate better recognition of malignant cells by surrounding immune cells. Therefore, to investigate the functional effects of our NTP-CIS combination, it is important to take into account the TME, especially the immune component.

Applied in this thesis, we used a 3D spheroid tumor model to include various crucial TME factors, including the ECM and multidimensional shape, promoting a gradient in nutritional factors and treatment exposure. Although this model enables a better *in vivo*-like representation and is thus more translatable to clinic, the model lacks cellular heterogeneity, including the absence of immune cells. Nonetheless, during this thesis, we improved this shortcoming by implementation of the immune component via DC co-culture experiments.

We supplemented DCs, isolated from donor-derived buffy-coats, HNSCC spheroids pre-treated with our NTP-CIS combination, to determine the therapeutic effects on tumor cell engulfment, processing, and maturation. After visual assessment of enhanced tumor cell uptake following NTP-CIS combination strategy (Figure 15), we quantitatively confirmed this with a flowcytometric analysis (Figure 16). Collectively, DC co-culture results demonstrated elevated phagocytotic capacity after NTP-CIS combination. Besides this, our results proposed an NTP-boosting impact on the activation and maturation stages of DCs. It is important to note that the DC populations are donor-dependent. Due to this variability, we were not able to identify significant differences in maturation and activation markers; although, the comparison of mean values showed the enhancing role of NTP. Altogether, the robust significance in DC phagocytosis across all cell lines and the general upregulated trend in

expressed maturation markers imply, besides increased DAMP release, also a functional improvement of tumor cell recognition and increased immune activation after NTP-CIS therapy.

One step further, our study validated the NTP-CIS combination therapy in a HNSCC organoid model, recently introduced in our lab. This 'patient-in-the-lab' model represents the real tumoral environment, maintaining both genotypic (e.g., mutational landscape) and phenotypic (e.g., cellular framework) characteristics of the patient's tumor. Hence, it is seen as a valuable and highly-advanced model to study biological processes, and to predict an individual patient's therapy response^[136]. Our lab has recently specialized itself in organoid research: with (1) development of a diverse organoid biobank, (2) an upscaled treatment method enabling proper NTP application and drug screening, and (3) an in-house developed analysis platform, OrBITS. Hence, we provided a strong tool for clinically relevant validation of (combinatorial) therapeutics and high-throughput screens for various treatment modalities in the future. Underlying this relevance, Millen et al. demonstrated very recently, and for the first time, a correlation in radiotherapy response between the HNSCC organoid model and the patient-resident tumor^[146], holding potential to guide treatment-related decisions and extension of personalized medicine. In regard of this predicting value, we added this appealing tool to our NTP-CIS validation pipeline.

By carrying out this thesis, we have paved the way to apply NTP-CIS treatment for the first time in a combinatorial design in an *in vivo* setting. Overall, our *in vitro* results demonstrated the attractive opportunity to combine emerging NTP with the first-line HNSCC treatment CIS to amplify immunogenic properties. Therefore, mouse experiments are planned to validate both safety and clinical efficacy of the NTP-CIS combination therapy *in vivo*. A suitable fully immunocompetent murine model, widely used in HNSCC, is the syngeneic C3H/HeN model^[147]. The SCC7 mouse-derived cell line will be injected orthotopically, in which tumor growth will be located in the original tumor site. In this respect, this model provides the best link with the TME, and displays similar HNSCC features compared to the human disease, like invasion in connective or muscular tissues and bone erosion^[147]. By this, a better insight of therapy efficacy and immunogenicity will be obtained in a complete biological system with key information on TME modulations. Since ICI is clinically often implemented in combination strategies^[143], it is highly relevant for further research to test a triple combination therapy of these checkpoint inhibitors with our studied NTP-CIS combination. This will further delineate the value of NTP as treatment addition to the current stand-of-care for R/M HNSCC.

Our findings opened several paths for further research in therapeutic triggering of the natural immune system to strengthen its capacity to eradicate malignant cells. With our innovative combination of NTP and CIS, we focused on targeting ER-mediated cellular stress mechanisms and the intracellular redox balance, with ICD induction as a mean to stimulate tumor immunogenicity. In parallel, other therapeutic strategies to retrieve immune stimulation are studied: breakthrough-approaches such as anti-cancer DC vaccines or chimeric antigen receptor therapy (CAR-T) are designed for specific targeting of tumor Ags, increasing the therapeutic efficacy and specificity, to reduce adverse effects. Nevertheless, they are time-consuming and still require high-cost development^[148]. Furthermore, TME is a strong immunosuppressive environment, including tumor hypoxia and acidification, counteracting many aspects of these immunotherapeutic agents. In that regard, tumor metabolism is a key target for cancer therapy which is currently underexplored. As NTP is reported to overload intracellular RONS mechanisms, thereby deregulating the redox metabolism of cancer cells, novel combinatorial approaches of NTP with metabolic agents may hold potential to target malignant metabolic rewiring as a novel immuno-metabolic strategy to improve cancer therapy.

Looking over the work done, it can be said that we were able to provide valuable insights in HNSCC immunogenicity after NTP-CIS combination therapy. First data on ICD markers generally showed NTP sensitization among all HNSCC cell lines, and greater DAMP release after combined application of NTP and CIS. Hereafter, evaluation of immune functionality demonstrated overall higher DC phagocytotic capacity and upregulation of maturation markers, boosting antigen presentation and subsequent recognition by the adaptive immunity. In this way, heightened tumor immunogenicity has the potential to trigger a durable anti-tumoral response. This all together will accelerate clinical translation of the obtained results and is a pivotal step towards a rationally designed combination strategy with NTP to improve current first line HNSCC therapies.

10 Supplementary Material

10.1 Organoid Medium

Ad-DF+++ medium consists of 500 mL Advanced DMEM (F12 12634, Life Technologies™) with 5 mL pen/strep (15140, Life Technologies™), 5 mL 1M Hepes (15630056, Life Technologies™), and 5 mL Glutamax (35050, Life Technologies™). The additionally 12 supplements are listed below (Table 3)

Table 3. The 12 supplements added for fully supplemented organoid medium.

	Cat nr	Supplier	Solvent	Weight	MM	Stock concentration	Dilution	Working concentration	10 mL
Ad-DF+++									8 mL
RSPO								4%	1 mL
Noggin								4%	1 mL
B27 supplement (-20°C, protect from light)	17504-044	Gibco				10ml	50x	1x	200 µL
N-acetylcysteine (NAC)	A9165-5g	Sigma	H ₂ O	5g	163.19	500 mM = 81.6 mg/ml	400x	1.25 mM	25 µL
Nicotinamide	N0636-100G	Sigma	H ₂ O	100g	122.12	1M	100x	10 mM	100 µL
A83-01	2939	Tocris Sigma 5mg	DMSO	5mg	421.52	500 µM	1000x	500 nM	10 µL
FGF-2*	100-18B	Peprotech		50 µg		50 µg/mL		5 ng/mL	1 µL
FGF-10	100-26	Peprotech	0.1% BSA/PBS	50 µg		100 µg/mL		10 ng/mL	1 µL
EGF	AF-100-15	Peprotech	0.1% BSA/ultra pure H ₂ O	1mg		500µg/ml		50 ng/ml	1 µL
Prostaglandin E2	2296	Tocris Bioscience	DMSO	10mg	352.47	10mM		1 µM	1 µL
CHIR 99021*	SML1046	Sigma	DMSO	5mg	465.34	1200 µM		3 µM	25 µL
Forskolin*	1099	Bio-Techne (R&D systems)	DMSO		MW depends on batch	10mM		1 µM	1 µL

11 Literature references

1. Organization W-WH. **Cancer - key facts**. WHO 2023.
2. Debela DT, Muzazu SG, Heraro KD, Ndalama MT, Mesele BW, Haile DC, et al. **New approaches and procedures for cancer treatment: Current perspectives**. *SAGE Open Med* 2021; 9:20503121211034366.
3. insitute Nc. **NCI Dictionary of Cancer Terms - conventional treatment**.
4. Ferlay J, Colombet M, Soerjomataram I, Parkin DM, Pineros M, Znaor A, et al. **Cancer statistics for the year 2020: An overview**. *Int J Cancer* 2021.
5. Gormley M, Creaney G, Schache A, Ingarfield K, Conway DI. **Reviewing the epidemiology of head and neck cancer: definitions, trends and risk factors**. *Br Dent J* 2022; 233(9):780-786.
6. Sung H, Ferlay J, Siegel RL, Laversanne M, Soerjomataram I, Jemal A, et al. **Global Cancer Statistics 2020: GLOBOCAN Estimates of Incidence and Mortality Worldwide for 36 Cancers in 185 Countries**. *CA Cancer J Clin* 2021; 71(3):209-249.
7. (WHO) WHO. **Estimated number of new cases from 2020 to 2040**. 2020.
8. Carvalho AL, Nishimoto IN, Califano JA, Kowalski LP. **Trends in incidence and prognosis for head and neck cancer in the United States: a site-specific analysis of the SEER database**. *Int J Cancer* 2005; 114(5):806-816.
9. Johnson DE, Burtneß B, Leemans CR, Lui VWY, Bauman JE, Grandis JR. **Head and neck squamous cell carcinoma**. *Nat Rev Dis Primers* 2020; 6(1):92.
10. Clinic C. **Head and Neck cancer - symptoms and causes**. 2022.
11. Driehuis E, Kolders S, Spelier S, Lohmussaar K, Willems SM, Devriese LA, et al. **Oral Mucosal Organoids as a Potential Platform for Personalized Cancer Therapy**. *Cancer Discov* 2019; 9(7):852-871.
12. Jose J, Coatesworth AP, Johnston C, MacLennan K. **Cervical node metastases in squamous cell carcinoma of the upper aerodigestive tract: the significance of extracapsular spread and soft tissue deposits**. *Head Neck* 2003; 25(6):451-456.
13. Cuffari L, Tesseroli de Siqueira JT, Nemr K, Rapaport A. **Pain complaint as the first symptom of oral cancer: a descriptive study**. *Oral Surg Oral Med Oral Pathol Oral Radiol Endod* 2006; 102(1):56-61.
14. Al-Rawi NH, Talabani NG. **Squamous cell carcinoma of the oral cavity: a case series analysis of clinical presentation and histological grading of 1,425 cases from Iraq**. *Clin Oral Investig* 2008; 12(1):15-18.
15. Shephard EA, Parkinson MA, Hamilton WT. **Recognising laryngeal cancer in primary care: a large case-control study using electronic records**. *Br J Gen Pract* 2019; 69(679):e127-e133.
16. Jamal Z, Anjum F. **Oropharyngeal Squamous Cell Carcinoma**. In: *StatPearls*. Treasure Island (FL); 2022.
17. Hashibe M, Brennan P, Chuang SC, Boccia S, Castellsague X, Chen C, et al. **Interaction between tobacco and alcohol use and the risk of head and neck cancer: pooled analysis in the International Head and Neck Cancer Epidemiology Consortium**. *Cancer Epidemiol Biomarkers Prev* 2009; 18(2):541-550.
18. Lin NC, Hsu JT, Tsai KY. **Difference between Female and Male Patients with Oral Squamous Cell Carcinoma: A Single-Center Retrospective Study in Taiwan**. *Int J Environ Res Public Health* 2020; 17(11).
19. Stein AP, Saha S, Kraninger JL, Swick AD, Yu M, Lambert PF, et al. **Prevalence of Human Papillomavirus in Oropharyngeal Cancer: A Systematic Review**. *Cancer J* 2015; 21(3):138-146.
20. Syrjanen K, Syrjanen S, Lamberg M, Pyrhonen S, Nuutinen J. **Morphological and immunohistochemical evidence suggesting human papillomavirus (HPV) involvement in oral squamous cell carcinogenesis**. *Int J Oral Surg* 1983; 12(6):418-424.
21. Schwartz SM, Daling JR, Doody DR, Wipf GC, Carter JJ, Madeleine MM, et al. **Oral cancer risk in relation to sexual history and evidence of human papillomavirus infection**. *J Natl Cancer Inst* 1998; 90(21):1626-1636.
22. Colin S Poon M, PhD, FRCPCR Kerstin M Stenson, MD, FACS. **Overview of the diagnosis and staging of head and neck cancer** *UpToDate* 2022.
23. Chaturvedi AK, Anderson WF, Lortet-Tieulent J, Curado MP, Ferlay J, Franceschi S, et al. **Worldwide trends in incidence rates for oral cavity and oropharyngeal cancers**. *J Clin Oncol* 2013; 31(36):4550-4559.
24. Ang KK, Harris J, Wheeler R, Weber R, Rosenthal DI, Nguyen-Tan PF, et al. **Human papillomavirus and survival of patients with oropharyngeal cancer**. *N Engl J Med* 2010; 363(1):24-35.
25. Gameiro SF, Evans AM, Mymryk JS. **The tumor immune microenvironments of HPV(+) and HPV(-) head and neck cancers**. *WIREs Mech Dis* 2022; 14(2):e1539.
26. Bradshaw PT, Siega-Riz AM, Campbell M, Weissler MC, Funkhouser WK, Olshan AF. **Associations between dietary patterns and head and neck cancer: the Carolina head and neck cancer epidemiology study**. *Am J Epidemiol* 2012; 175(12):1225-1233.
27. Chang JS, Lo HI, Wong TY, Huang CC, Lee WT, Tsai ST, et al. **Investigating the association between oral hygiene and head and neck cancer**. *Oral Oncol* 2013; 49(10):1010-1017.

28. Hashim D, Sartori S, La Vecchia C, Serraino D, Maso LD, Negri E, et al. **Hormone factors play a favorable role in female head and neck cancer risk.** *Cancer Med* 2017; 6(8):1998-2007.
29. Hashibe M, Hunt J, Wei M, Buys S, Gren L, Lee YC. **Tobacco, alcohol, body mass index, physical activity, and the risk of head and neck cancer in the prostate, lung, colorectal, and ovarian (PLCO) cohort.** *Head Neck* 2013; 35(7):914-922.
30. Auperin A. **Epidemiology of head and neck cancers: an update.** *Curr Opin Oncol* 2020; 32(3):178-186.
31. Hashim D, Genden E, Posner M, Hashibe M, Boffetta P. **Head and neck cancer prevention: from primary prevention to impact of clinicians on reducing burden.** *Ann Oncol* 2019; 30(5):744-756.
32. Gregoire V, Lefebvre JL, Licitra L, Felip E, Group E-E-EGW. **Squamous cell carcinoma of the head and neck: EHNS-ESMO-ESTRO Clinical Practice Guidelines for diagnosis, treatment and follow-up.** *Ann Oncol* 2010; 21 Suppl 5:v184-186.
33. Reyes-Gibby CC, Anderson KO, Merriman KW, Todd KH, Shete SS, Hanna EY. **Survival patterns in squamous cell carcinoma of the head and neck: pain as an independent prognostic factor for survival.** *J Pain* 2014; 15(10):1015-1022.
34. Bruce E Brockstein MMS, MD, FACSShiyu Song, MD, PhD. **Overview of treatment for head and neck cancer** *UpToDate* 2022.
35. Santos FMD, Viani GA, Pavoni JF. **Evaluation of survival of patients with locally advanced head and neck cancer treated in a single center.** *Braz J Otorhinolaryngol* 2021; 87(1):3-10.
36. Bruce E Brockstein MEV, MD. **Treatment of metastatic and recurrent head and neck cancer.** *UpToDate* 2022.
37. Lee YG, Kang EJ, Keam B, Choi JH, Kim JS, Park KU, et al. **Treatment strategy and outcomes in locally advanced head and neck squamous cell carcinoma: a nationwide retrospective cohort study (KCSG HN13-01).** *BMC Cancer* 2020; 20(1):813.
38. Harreus U. **Surgical errors and risks - the head and neck cancer patient.** *GMS Curr Top Otorhinolaryngol Head Neck Surg* 2013; 12:Doc04.
39. Shih HS, Zhou HJ, Ou YH, Liu YT, Kor CT, Chen AW, et al. **The Efficacy and Adverse Events in Patients with Head and Neck Cancer Following Radiotherapy Combined with S-1 Therapy: A Meta-Analysis.** *Cancers (Basel)* 2021; 13(12).
40. Goel B, Tiwari AK, Pandey RK, Singh AP, Kumar S, Sinha A, et al. **Therapeutic approaches for the treatment of head and neck squamous cell carcinoma-An update on clinical trials.** *Transl Oncol* 2022; 21:101426.
41. Nissi L, Suilamo S, Kytö E, Vaittinen S, Irjala H, Minn H. **Recurrence of head and neck squamous cell carcinoma in relation to high-risk treatment volume.** *Clin Transl Radiat Oncol* 2021; 27:139-146.
42. Corte-Rodriguez M, Espina M, Sierra LM, Blanco E, Ames T, Montes-Bayon M, et al. **Quantitative evaluation of cellular uptake, DNA incorporation and adduct formation in cisplatin sensitive and resistant cell lines: Comparison of different Pt-containing drugs.** *Biochem Pharmacol* 2015; 98(1):69-77.
43. Dasari S, Tchounwou PB. **Cisplatin in cancer therapy: molecular mechanisms of action.** *Eur J Pharmacol* 2014; 740:364-378.
44. Harrington KJ, Burtneß B, Greil R, Soulieres D, Tahara M, de Castro G, Jr., et al. **Pembrolizumab With or Without Chemotherapy in Recurrent or Metastatic Head and Neck Squamous Cell Carcinoma: Updated Results of the Phase III KEYNOTE-048 Study.** *J Clin Oncol* 2022:JCO2102508.
45. Burtneß B, Harrington KJ, Greil R, Soulieres D, Tahara M, de Castro G, Jr., et al. **Pembrolizumab alone or with chemotherapy versus cetuximab with chemotherapy for recurrent or metastatic squamous cell carcinoma of the head and neck (KEYNOTE-048): a randomised, open-label, phase 3 study.** *Lancet* 2019; 394(10212):1915-1928.
46. Garcia Sar D, Montes-Bayon M, Blanco Gonzalez E, Sierra Zapico LM, Sanz-Medel A. **Reduction of cisplatin-induced nephrotoxicity in vivo by selenomethionine: the effect on cisplatin-DNA adducts.** *Chem Res Toxicol* 2011; 24(6):896-904.
47. Lebwahl D, Canetta R. **Clinical development of platinum complexes in cancer therapy: an historical perspective and an update.** *Eur J Cancer* 1998; 34(10):1522-1534.
48. Rapoport BL, van Eeden R, Sibaud V, Epstein JB, Klastersky J, Aapro M, et al. **Supportive care for patients undergoing immunotherapy.** *Support Care Cancer* 2017; 25(10):3017-3030.
49. Bauml JM, Aggarwal C, Cohen RB. **Immunotherapy for head and neck cancer: where are we now and where are we going?** *Ann Transl Med* 2019; 7(Suppl 3):S75.
50. Ribas A, Hu-Lieskova S. **What does PD-L1 positive or negative mean?** *J Exp Med* 2016; 213(13):2835-2840.
51. Chaplin DD. **1. Overview of the human immune response.** *J Allergy Clin Immunol* 2006; 117(2 Suppl Mini-Primer):S430-435.

52. Houghton AN, Guevara-Patino JA. **Immune recognition of self in immunity against cancer.** *J Clin Invest* 2004; 114(4):468-471.
53. Aatman S, Doshi KHA. **Chapter Two - Innate and adaptive immunity in cancer.** 2022; 1:19-61.
54. Chen DS, Mellman I. **Oncology meets immunology: the cancer-immunity cycle.** *Immunity* 2013; 39(1):1-10.
55. Al-Ashmawy GMZ. **Dendritic Cell Subsets, Maturation and Function.** 2018.
56. Aerts-Toegaert C, Heirman C, Tuyaeerts S, Corthals J, Aerts JL, Bonehill A, et al. **CD83 expression on dendritic cells and T cells: correlation with effective immune responses.** *Eur J Immunol* 2007; 37(3):686-695.
57. Hanahan D, Weinberg RA. **The hallmarks of cancer.** *Cell* 2000; 100(1):57-70.
58. Hanahan D, Weinberg RA. **Hallmarks of cancer: the next generation.** *Cell* 2011; 144(5):646-674.
59. Hanahan D. **Hallmarks of Cancer: New Dimensions.** *Cancer Discov* 2022; 12(1):31-46.
60. Moy JD, Moskovitz JM, Ferris RL. **Biological mechanisms of immune escape and implications for immunotherapy in head and neck squamous cell carcinoma.** *Eur J Cancer* 2017; 76:152-166.
61. Ogino T, Shigyo H, Ishii H, Katayama A, Miyokawa N, Harabuchi Y, et al. **HLA class I antigen down-regulation in primary laryngeal squamous cell carcinoma lesions as a poor prognostic marker.** *Cancer Res* 2006; 66(18):9281-9289.
62. Mariathasan S, Turley SJ, Nickles D, Castiglioni A, Yuen K, Wang Y, et al. **TGFbeta attenuates tumour response to PD-L1 blockade by contributing to exclusion of T cells.** *Nature* 2018; 554(7693):544-548.
63. Chang CH, Curtis JD, Maggi LB, Jr., Faubert B, Villarino AV, O'Sullivan D, et al. **Posttranscriptional control of T cell effector function by aerobic glycolysis.** *Cell* 2013; 153(6):1239-1251.
64. Tormoen GW, Crittenden MR, Gough MJ. **Role of the immunosuppressive microenvironment in immunotherapy.** *Adv Radiat Oncol* 2018; 3(4):520-526.
65. Zhang Y, Ertl HC. **Starved and Asphyxiated: How Can CD8(+) T Cells within a Tumor Microenvironment Prevent Tumor Progression.** *Front Immunol* 2016; 7:32.
66. Anguille S, Smits EL, Lion E, van Tendeloo VF, Berneman ZN. **Clinical use of dendritic cells for cancer therapy.** *Lancet Oncol* 2014; 15(7):e257-267.
67. Smith PL, Piadel K, Dalgleish AG. **Directing T-Cell Immune Responses for Cancer Vaccination and Immunotherapy.** *Vaccines (Basel)* 2021; 9(12).
68. Galluzzi L, Vitale I, Aaronson SA, Abrams JM, Adam D, Agostinis P, et al. **Molecular mechanisms of cell death: recommendations of the Nomenclature Committee on Cell Death 2018.** *Cell Death Differ* 2018; 25(3):486-541.
69. Fucikova J, Kasikova L, Truxova I, Laco J, Skapa P, Ryska A, et al. **Relevance of the chaperone-like protein calreticulin for the biological behavior and clinical outcome of cancer.** *Immunol Lett* 2018; 193:25-34.
70. Zhou J, Wang G, Chen Y, Wang H, Hua Y, Cai Z. **Immunogenic cell death in cancer therapy: Present and emerging inducers.** *J Cell Mol Med* 2019; 23(8):4854-4865.
71. Khalili M, Daniels L, Lin A, Krebs FC, Snook AE, Bekeschus S, et al. **Non-Thermal Plasma-Induced Immunogenic Cell Death in Cancer: A Topical Review.** *J Phys D Appl Phys* 2019; 52(42).
72. Hernandez AP, Juanes-Velasco P, Landeira-Vinuela A, Bareke H, Montalvillo E, Gongora R, et al. **Restoring the Immunity in the Tumor Microenvironment: Insights into Immunogenic Cell Death in Onco-Therapies.** *Cancers (Basel)* 2021; 13(11).
73. Obeid M, Tesniere A, Ghiringhelli F, Fimia GM, Apetoh L, Perfettini JL, et al. **Calreticulin exposure dictates the immunogenicity of cancer cell death.** *Nat Med* 2007; 13(1):54-61.
74. Kepp O, Senovilla L, Vitale I, Vacchelli E, Adjemian S, Agostinis P, et al. **Consensus guidelines for the detection of immunogenic cell death.** *Oncoimmunology* 2014; 3(9):e955691.
75. Li W. **Eat-me signals: keys to molecular phagocyte biology and "appetite" control.** *J Cell Physiol* 2012; 227(4):1291-1297.
76. Genest O, Wickner S, Doyle SM. **Hsp90 and Hsp70 chaperones: Collaborators in protein remodeling.** *J Biol Chem* 2019; 294(6):2109-2120.
77. Adkins I, Sadilkova L, Hradilova N, Tomala J, Kovar M, Spisek R. **Severe, but not mild heat-shock treatment induces immunogenic cell death in cancer cells.** *Oncoimmunology* 2017; 6(5):e1311433.
78. Fucikova J, Kepp O, Kasikova L, Petroni G, Yamazaki T, Liu P, et al. **Detection of immunogenic cell death and its relevance for cancer therapy.** *Cell Death Dis* 2020; 11(11):1013.
79. Elliott MR, Chekeni FB, Trampont PC, Lazarowski ER, Kadl A, Walk SF, et al. **Nucleotides released by apoptotic cells act as a find-me signal to promote phagocytic clearance.** *Nature* 2009; 461(7261):282-286.
80. Yang H, Wang H, Chavan SS, Andersson U. **High Mobility Group Box Protein 1 (HMGB1): The Prototypical Endogenous Danger Molecule.** *Mol Med* 2015; 21 Suppl 1(Suppl 1):S6-S12.
81. Park JS, Gamboni-Robertson F, He Q, Svetkauskaite D, Kim JY, Strassheim D, et al. **High mobility group box 1 protein interacts with multiple Toll-like receptors.** *Am J Physiol Cell Physiol* 2006; 290(3):C917-924.

82. Golden EB, Frances D, Pellicciotta I, Demaria S, Helen Barcellos-Hoff M, Formenti SC. **Radiation fosters dose-dependent and chemotherapy-induced immunogenic cell death.** *Oncoimmunology* 2014; 3:e28518.
83. Hodge JW, Garnett CT, Farsaci B, Palena C, Tsang KY, Ferrone S, et al. **Chemotherapy-induced immunogenic modulation of tumor cells enhances killing by cytotoxic T lymphocytes and is distinct from immunogenic cell death.** *Int J Cancer* 2013; 133(3):624-636.
84. Park SJ, Ye W, Xiao R, Silvin C, Padgett M, Hodge JW, et al. **Cisplatin and oxaliplatin induce similar immunogenic changes in preclinical models of head and neck cancer.** *Oral Oncol* 2019; 95:127-135.
85. Wang X, Wu S, Liu F, Ke D, Wang X, Pan D, et al. **An Immunogenic Cell Death-Related Classification Predicts Prognosis and Response to Immunotherapy in Head and Neck Squamous Cell Carcinoma.** *Front Immunol* 2021; 12:781466.
86. Birmipilis AI, Paschalis A, Mourkakis A, Christodoulou P, Kostopoulos IV, Antimissari E, et al. **Immunogenic Cell Death, DAMPs and Prothymosin alpha as a Putative Anticancer Immune Response Biomarker.** *Cells* 2022; 11(9).
87. Lin A, Gorbanev Y, De Backer J, Van Loenhout J, Van Boxem W, Lemiere F, et al. **Non-Thermal Plasma as a Unique Delivery System of Short-Lived Reactive Oxygen and Nitrogen Species for Immunogenic Cell Death in Melanoma Cells.** *Adv Sci (Weinh)* 2019; 6(6):1802062.
88. Lin AG, Xiang B, Merlino DJ, Baybutt TR, Sahu J, Fridman A, et al. **Non-thermal plasma induces immunogenic cell death in vivo in murine CT26 colorectal tumors.** *Oncoimmunology* 2018; 7(9):e1484978.
89. Yan D, Sherman JH, Keidar M. **Cold atmospheric plasma, a novel promising anti-cancer treatment modality.** *Oncotarget* 2017; 8(9):15977-15995.
90. Keidar M, Yan D, Beilis, II, Trink B, Sherman JH. **Plasmas for Treating Cancer: Opportunities for Adaptive and Self-Adaptive Approaches.** *Trends Biotechnol* 2018; 36(6):586-593.
91. P André YAB, G Faure and S M Shkol'nik. **Characteristics of discharge with liquid non-metallic cathode burning in air flow.** *Journal of Physics D: Applied Physics* 2018.
92. Lu X, Laroussi M, Puech V. **On atmospheric-pressure non-equilibrium plasma jets and plasma bullets.** *Plasma Sources Sci T* 2012; 21(3).
93. Lin A, Truong B, Patel S, Kaushik N, Choi EH, Fridman G, et al. **Nanosecond-Pulsed DBD Plasma-Generated Reactive Oxygen Species Trigger Immunogenic Cell Death in A549 Lung Carcinoma Cells through Intracellular Oxidative Stress.** *Int J Mol Sci* 2017; 18(5).
94. Kang SU, Cho JH, Chang JW, Shin YS, Kim KI, Park JK, et al. **Nonthermal plasma induces head and neck cancer cell death: the potential involvement of mitogen-activated protein kinase-dependent mitochondrial reactive oxygen species.** *Cell Death Dis* 2014; 5(2):e1056.
95. Guerrero-Preston R, Ogawa T, Uemura M, Shumulinsky G, Valle BL, Pirini F, et al. **Cold atmospheric plasma treatment selectively targets head and neck squamous cell carcinoma cells.** *Int J Mol Med* 2014; 34(4):941-946.
96. Liedtke KR, Bekeschus S, Kaeding A, Hackbarth C, Kuehn JP, Heidecke CD, et al. **Non-thermal plasma-treated solution demonstrates antitumor activity against pancreatic cancer cells in vitro and in vivo.** *Sci Rep* 2017; 7(1):8319.
97. Lin L, Wang L, Liu Y, Xu C, Tu Y, Zhou J. **Non-thermal plasma inhibits tumor growth and proliferation and enhances the sensitivity to radiation in vitro and in vivo.** *Oncol Rep* 2018; 40(6):3405-3415.
98. Hans-Robert Metelmann CS, Vandana Miller, Alexander Fridman, Georg Bauer, David B.Graves, Jean-Michel Pouvesle, Rico Rutkowski, Matthias Schuster, Sander Bekeschus, Kristian Wende, Kai Masur, Sybille Hasse, Torsten Gerling, Masaru Hori, HiromasaTanaka, Eun Ha Choi, Klaus-Dieter Weltmann, Philine Henriette, Metelmann,Daniel D.Von Hoff, Thomas von Woedtke. **Clinical experience with cold plasma in the treatment of locally advanced head and neck cancer.** *Elsevier* 2018; 9:6-13.
99. Abraham Lin BT, Gregory Fridman, Alexander Fridman, & Vandana Miller*. **Immune Cells Enhance Selectivity of Nanosecond-Pulsed DBD Plasma Against Tumor Cells.** *Plasma Medicine* 2017.
100. Trachootham D, Alexandre J, Huang P. **Targeting cancer cells by ROS-mediated mechanisms: a radical therapeutic approach?** *Nat Rev Drug Discov* 2009; 8(7):579-591.
101. Kim SJ, Chung TH. **Cold atmospheric plasma jet-generated RONS and their selective effects on normal and carcinoma cells.** *Sci Rep* 2016; 6:20332.
102. Valko M, Leibfritz D, Moncol J, Cronin MT, Mazur M, Telser J. **Free radicals and antioxidants in normal physiological functions and human disease.** *Int J Biochem Cell Biol* 2007; 39(1):44-84.
103. Kaushik N, Uddin N, Sim GB, Hong YJ, Baik KY, Kim CH, et al. **Responses of solid tumor cells in DMEM to reactive oxygen species generated by non-thermal plasma and chemically induced ROS systems.** *Sci Rep* 2015; 5:8587.

104. Simon HU, Haj-Yehia A, Levi-Schaffer F. **Role of reactive oxygen species (ROS) in apoptosis induction.** *Apoptosis* 2000; 5(5):415-418.
105. Weinberg F, Hamanaka R, Wheaton WW, Weinberg S, Joseph J, Lopez M, et al. **Mitochondrial metabolism and ROS generation are essential for Kras-mediated tumorigenicity.** *Proc Natl Acad Sci U S A* 2010; 107(19):8788-8793.
106. Brulle L, Vandamme M, Ries D, Martel E, Robert E, Lerondel S, et al. **Effects of a non thermal plasma treatment alone or in combination with gemcitabine in a MIA PaCa2-luc orthotopic pancreatic carcinoma model.** *PLoS One* 2012; 7(12):e52653.
107. Chang JW, Kang SU, Shin YS, Seo SJ, Kim YS, Yang SS, et al. **Combination of NTP with cetuximab inhibited invasion/migration of cetuximab-resistant OSCC cells: Involvement of NF-kappaB signaling.** *Sci Rep* 2015; 5:18208.
108. Bugaut H, Bruchard M, Berger H, Derangere V, Odoul L, Euvrard R, et al. **Bleomycin exerts ambivalent antitumor immune effect by triggering both immunogenic cell death and proliferation of regulatory T cells.** *PLoS One* 2013; 8(6):e65181.
109. Tinhofer I, Braunholz D, Klinghammer K. **Preclinical models of head and neck squamous cell carcinoma for a basic understanding of cancer biology and its translation into efficient therapies.** *Cancers Head Neck* 2020; 5:9.
110. Kapalczyńska M, Kolenda T, Przybyła W, Zajackowska M, Teresiak A, Filas V, et al. **2D and 3D cell cultures - a comparison of different types of cancer cell cultures.** *Arch Med Sci* 2018; 14(4):910-919.
111. Ryan JA. **Introduction to animal cell culture.** *Technical Bulletin* 2008.
112. Langhans SA. **Three-Dimensional in Vitro Cell Culture Models in Drug Discovery and Drug Repositioning.** *Front Pharmacol* 2018; 9:6.
113. Wang M, Zhao J, Zhang L, Wei F, Lian Y, Wu Y, et al. **Role of tumor microenvironment in tumorigenesis.** *J Cancer* 2017; 8(5):761-773.
114. Breslin S, O'Driscoll L. **Three-dimensional cell culture: the missing link in drug discovery.** *Drug Discov Today* 2013; 18(5-6):240-249.
115. Melissaridou S, Wiechec E, Magan M, Jain MV, Chung MK, Farnebo L, et al. **The effect of 2D and 3D cell cultures on treatment response, EMT profile and stem cell features in head and neck cancer.** *Cancer Cell Int* 2019; 19:16.
116. Begley CG, Ellis LM. **Drug development: Raise standards for preclinical cancer research.** *Nature* 2012; 483(7391):531-533.
117. Chen F, Zhuang X, Lin L, Yu P, Wang Y, Shi Y, et al. **New horizons in tumor microenvironment biology: challenges and opportunities.** *BMC Med* 2015; 13:45.
118. Brassart-Pasco S, Brezillon S, Brassart B, Ramont L, Oudart JB, Monboisse JC. **Tumor Microenvironment: Extracellular Matrix Alterations Influence Tumor Progression.** *Front Oncol* 2020; 10:397.
119. Bonnans C, Chou J, Werb Z. **Remodelling the extracellular matrix in development and disease.** *Nat Rev Mol Cell Biol* 2014; 15(12):786-801.
120. Duval K, Grover H, Han LH, Mou Y, Pegoraro AF, Fredberg J, et al. **Modeling Physiological Events in 2D vs. 3D Cell Culture.** *Physiology (Bethesda)* 2017; 32(4):266-277.
121. Ryan SL, Baird AM, Vaz G, Urquhart AJ, Senge M, Richard DJ, et al. **Drug Discovery Approaches Utilizing Three-Dimensional Cell Culture.** *Assay Drug Dev Technol* 2016; 14(1):19-28.
122. Koch J, Monch D, Maass A, Gromoll C, Hehr T, Leibold T, et al. **Three dimensional cultivation increases chemo- and radioresistance of colorectal cancer cell lines.** *PLoS One* 2021; 16(1):e0244513.
123. Franco OE, Shaw AK, Strand DW, Hayward SW. **Cancer associated fibroblasts in cancer pathogenesis.** *Semin Cell Dev Biol* 2010; 21(1):33-39.
124. Canning M, Guo G, Yu M, Myint C, Groves MW, Byrd JK, et al. **Heterogeneity of the Head and Neck Squamous Cell Carcinoma Immune Landscape and Its Impact on Immunotherapy.** *Front Cell Dev Biol* 2019; 7:52.
125. Edmondson R, Broglie JJ, Adcock AF, Yang L. **Three-dimensional cell culture systems and their applications in drug discovery and cell-based biosensors.** *Assay Drug Dev Technol* 2014; 12(4):207-218.
126. Chen SMY, Krinsky AL, Woolaver RA, Wang X, Chen Z, Wang JH. **Tumor immune microenvironment in head and neck cancers.** *Mol Carcinog* 2020; 59(7):766-774.
127. Weiswald LB, Bellet D, Dangles-Marie V. **Spherical cancer models in tumor biology.** *Neoplasia* 2015; 17(1):1-15.
128. Lv D, Hu Z, Lu L, Lu H, Xu X. **Three-dimensional cell culture: A powerful tool in tumor research and drug discovery.** *Oncol Lett* 2017; 14(6):6999-7010.

129. Kadletz L, Heiduschka G, Domayer J, Schmid R, Enzenhofer E, Thurnher D. **Evaluation of spheroid head and neck squamous cell carcinoma cell models in comparison to monolayer cultures.** *Oncol Lett* 2015; 10(3):1281-1286.
130. Mery B, Rancoule C, Guy JB, Espenel S, Wozny AS, Battiston-Montagne P, et al. **Preclinical models in HNSCC: A comprehensive review.** *Oral Oncol* 2017; 65:51-56.
131. Miebach L, Freund E, Horn S, Niessner F, Sagwal SK, von Woedtke T, et al. **Tumor cytotoxicity and immunogenicity of a novel V-jet neon plasma source compared to the kINPen.** *Sci Rep* 2021; 11(1):136.
132. Krysko DV, Demuyneck R, Efimova I, Naessens F, Krysko O, Catanzaro E. **In Vitro Veritas: From 2D Cultures to Organ-on-a-Chip Models to Study Immunogenic Cell Death in the Tumor Microenvironment.** *Cells* 2022; 11(22).
133. Courau T, Bonnereau J, Chicoteau J, Bottois H, Remark R, Assante Miranda L, et al. **Cocultures of human colorectal tumor spheroids with immune cells reveal the therapeutic potential of MICA/B and NKG2A targeting for cancer treatment.** *J Immunother Cancer* 2019; 7(1):74.
134. Saraiva DP, Matias AT, Braga S, Jacinto A, Cabral MG. **Establishment of a 3D Co-culture With MDA-MB-231 Breast Cancer Cell Line and Patient-Derived Immune Cells for Application in the Development of Immunotherapies.** *Front Oncol* 2020; 10:1543.
135. Kross KW, Heimdal JH, Olsnes C, Olofsson J, Aarstad HJ. **Co-culture of head and neck squamous cell carcinoma spheroids with autologous monocytes predicts prognosis.** *Scand J Immunol* 2008; 67(4):392-399.
136. Deben C, De La Hoz EC, Compte ML, Van Schil P, Hendriks JMH, Lauwers P, et al. **OrBITS: label-free and time-lapse monitoring of patient derived organoids for advanced drug screening.** *Cell Oncol (Dordr)* 2023; 46(2):299-314.
137. Vlachogiannis G, Hedayat S, Vatsiou A, Jamin Y, Fernandez-Mateos J, Khan K, et al. **Patient-derived organoids model treatment response of metastatic gastrointestinal cancers.** *Science* 2018; 359(6378):920-926.
138. Abraham Lin BT, Arthur Pappas, Lawrence Kirifides, Ahmed Oubbari, Shuyang Chen, Shaojun Lin, Danil Dobrynin, Gregory Fridman, Alexander Fridman, Nianli Sang, Vandana Miller*. **Uniform Nanosecond Pulsed Dielectric Barrier Discharge Plasma Enhances Anti-Tumor Effects by Induction of Immunogenic Cell Death in Tumors and Stimulation of Macrophages.** 2015.
139. Berghmans E, Jacobs J, Deben C, Hermans C, Broeckx G, Smits E, et al. **Mass Spectrometry Imaging Reveals Neutrophil Defensins as Additional Biomarkers for Anti-PD-(L)1 Immunotherapy Response in NSCLC Patients.** *Cancers (Basel)* 2020; 12(4).
140. Nguyen MT, Schellerhoff LH, Niemann S, Schaumburg F, Herrmann M. **Quiescence of Human Monocytes after Affinity Purification: A Novel Method Apt for Monocyte Stimulation Assays.** *Biomolecules* 2022; 12(3).
141. Rajkumar P, Mathew BS, Das S, Isaiah R, John S, Prabha R, et al. **Cisplatin Concentrations in Long and Short Duration Infusion: Implications for the Optimal Time of Radiation Delivery.** *J Clin Diagn Res* 2016; 10(7):XC01-XC04.
142. Sasaya T, Kubo T, Murata K, Mizue Y, Sasaki K, Yanagawa J, et al. **Cisplatin-induced HSF1-HSP90 axis enhances the expression of functional PD-L1 in oral squamous cell carcinoma.** *Cancer Med* 2023; 12(4):4605-4615.
143. Tsutsumi H, Inoue H, Shiraishi Y, Hirayama A, Nakanishi T, Ando H, et al. **Impact of increased plasma levels of calreticulin on prognosis of patients with advanced lung cancer undergoing combination treatment of chemotherapy and immune checkpoint inhibitors.** *Lung Cancer* 2023; 181:107264.
144. Chavez-Dominguez RL, Perez-Medina MA, Lopez-Gonzalez JS, Galicia-Velasco M, Matias-Florentino M, Avila-Rios S, et al. **Role of HMGB1 in Cisplatin-Persistent Lung Adenocarcinoma Cell Lines.** *Front Oncol* 2021; 11:750677.
145. Kang R, Chen R, Zhang Q, Hou W, Wu S, Cao L, et al. **HMGB1 in health and disease.** *Mol Aspects Med* 2014; 40:1-116.
146. Millen R, De Kort WWB, Koomen M, van Son GJF, Gobits R, Penning de Vries B, et al. **Patient-derived head and neck cancer organoids allow treatment stratification and serve as a tool for biomarker validation and identification.** *Med* 2023; 4(5):290-310 e212.
147. Vahle AK, Kerem A, Ozturk E, Bankfalvi A, Lang S, Brandau S. **Optimization of an orthotopic murine model of head and neck squamous cell carcinoma in fully immunocompetent mice--role of toll-like-receptor 4 expressed on host cells.** *Cancer Lett* 2012; 317(2):199-206.
148. Society TAC. **How Immunotherapy Is Used to Treat Cancer.** 2019.